Neurobiology of Aging 56 (2017) 50–66

Contents lists available at ScienceDirect

Neurobiology of Aging

journal homepage: www.elsevier.com/locate/neuaging

Neuronal tetraploidization in the cerebral cortex correlates with reduced cognition in mice and precedes and recapitulates Alzheimer's-associated neuropathology

Noelia López-Sánchez [a,b], Ángela Fontán-Lozano [a], Anna Pallé [a], Valentina González-Álvarez [c], Alberto Rábano [c], José L. Trejo [a], José M. Frade [a,*]

[a] Department of Molecular, Cellular and Developmental Neurobiology, Cajal Institute, IC-CSIC, Madrid, Spain
[b] Tetraneuron S.L., Valencia, Spain
[c] Department of Neuropathology and Tissue Bank, Fundación CIEN, Instituto de Salud Carlos III, Madrid, Spain

ARTICLE INFO

Article history:
Received 10 September 2016
Received in revised form 28 March 2017
Accepted 9 April 2017
Available online 18 April 2017

Keywords:
E2F1
Memory
β-Amyloid
Flow cytometry
FISH
DNA content

ABSTRACT

A controversy exists as to whether de novo-generated neuronal tetraploidy (dnNT) occurs in Alzheimer's disease. In addition, the presence of age-associated dnNT in the normal brain remains unexplored. Here we show that age-associated dnNT occurs in both superficial and deep layers of the cerebral cortex of adult mice, a process that is blocked in the absence of E2F1, a known regulator of cell cycle progression. This blockage correlates with improved cognition despite compromised neurogenesis in the adult hippocampus was confirmed in mice lacking the *E2f1* gene. We also show that the human cerebral cortex contains tetraploid neurons. In normal humans, age-associated dnNT specifically occurs in the entorhinal cortex whereas, in Alzheimer, dnNT also affects association cortices prior to neurofibrillary tangle formation. Alzheimer-associated dnNT is likely potentiated by altered amyloid precursor protein (APP) processing as it is enhanced in the cerebral cortex of young $APP^{swe}/PS1^{deltaE9}$ mice, long before the first amyloid plaques are visible in their brains. In contrast to age-associated dnNT, enhanced dnNT in $APP^{swe}/PS1^{deltaE9}$ mice mostly affects the superficial cortical layers. The correlation of dnNT with reduced cognition in mice and its spatiotemporal course, preceding and recapitulating Alzheimer-associated neuropathology, makes this process a potential target for intervention in Alzheimer's disease.

1. Introduction

Alzheimer's disease (AD) is the most prevalent cause of dementia in the elderly (Brookmeyer et al., 1998). This condition is characterized by neuronal degeneration, accompanied by the alteration of spatiotemporal perception as well as of other higher brain functions, including memory and language skills (Förstl and Kurz, 1999). From a neuropathological view, AD presents 2 types of histological lesions (Markesbery, 1997): extracellular deposits of β-amyloid (Aβ) peptide (i.e., senile plaques [SPs]), mostly constituted by its pathological form: $Aβ_{1-42}$, and intracellular aggregates composed by hyperphosphorylated forms of Tau protein (i.e., neurofibrillary tangles [NFTs]). Both lesions spread throughout the brain following a stereotyped pattern. NFTs first appear in the entorhinal cortex (EC; Braak stages I/II), and then they spread toward limbic structures (including the hippocampus; Braak stages III/IV), and association cortices (Braak stages V/VI), as the disease evolves (Braak and Braak, 1991). In contrast, SPs spread from association cortices (Thal phase 1) to allocortical areas (including the EC and hippocampus) at Thal phase 2, and from there to diencephalic nuclei, striatum, and cholinergic nuclei of the basal forebrain areas (Thal phase 3), several brain stem nuclei (Thal phase 4), and cerebellum (Thal phase 5) (Thal et al., 2000, 2002).

There are many reports in the literature showing that cell cycle reactivation in neurons represents an early alteration associated with AD (Ding et al., 2000; Smith and Lippa, 1995; Tomashevski et al., 2001; Vincent et al., 1998, 2001). These observations are consistent with the expression in the affected neurons of key S-phase regulators including cyclin D/Cdk4 (Busser et al., 1998; Hoozemans et al., 2002; McShea et al., 1997; Yang et al., 2003), E2F1 and hyperphosphorylated retinoblastoma (Jordan-Sciutto et al., 2002; Thakur et al., 2008), and cyclin E/cdk2 (Hoozemans et al., 2002; Nagy et al., 1997; Sultana and Butterfield, 2007). Neurons that reactivate the cell cycle are rarely observed to undergo

* Corresponding author at: Department of Molecular, Cellular and Developmental Neurobiology, Cajal Institute, CSIC, Avenida Doctor Arce 37, 28002 Madrid, Spain. Tel.: +34-91-5854740; fax: +34-91-5854754.
E-mail address: frade@cajal.csic.es (J.M. Frade).

0197-4580/$ – see front matter © 2017 Elsevier Inc. All rights reserved.
http://dx.doi.org/10.1016/j.neurobiolaging.2017.04.008

mitosis (Bowser and Smith, 2002), and they likely remain as tetraploid cells (Mosch et al., 2007; Yang et al., 2001) that undergo delayed cell death at later stages of AD (Arendt et al., 2010; Busser et al., 1998; Yang et al., 2001, 2003). In contrast with these latter studies, Westra et al. (2009) were unable to detect tetraploid neurons in the Alzheimer brain. It is crucial therefore to verify whether de novo-generated neuronal tetraploidy (dnNT) occurs in Alzheimer, as the presence of double amount of DNA in neurons might participate in the etiology of this devastating disease (Frade and López-Sánchez, 2010). If dnNT can be found in the Alzheimer-affected brain, it is likely that the uncovering of the mechanism that regulates this process, the neurons that become affected, and the pathophysiological effects of dnNT, will facilitate the development of therapeutical strategies against this neurodegenerative disorder.

dnNT in the adult brain might be reminiscent of a normal process of neuronal tetraploidization taking place in the developing brain. In this regard, we and others have demonstrated that during development, some populations of differentiating neurons duplicate their genome as they migrate to their specific layers, and remain with tetraploid DNA content in the adult nervous system (López-Sánchez and Frade, 2013a; Morillo et al., 2010; Shirazi Fard et al., 2013, 2014). These tetraploid neurons are functional (López-Sánchez and Frade, 2013a) and, in the retina, they constitute specific populations with enlarged cell body and extensive dendrites, innervating defined target areas (Morillo et al., 2010). Neuronal tetraploidization during development takes place in E2F1-expressing neuroblasts through a developmental program that requires $p75^{NTR}$ activity, which leads to E2F4 phosphorylation by $p38^{MAPK}$ (López-Sánchez and Frade, 2013a; Morillo et al., 2010, 2012).

In this study, we have explored the possibility that the deregulation of the mechanisms controlling DNA replication in differentiating neurons might participate in pathological dnNT. We have found that dnNT can be detected in the cerebral cortex of normal individuals, taking place in an age- and tissue-dependent fashion. In mice, age-associated dnNT in the cerebral cortex is regulated by E2F1 and its blockade correlates with cognitive enhancement. We also found that dnNT is potentiated in $APP^{swe}/PS1^{deltaE9}$ (APP/PS1) mice and, in AD patients, precedes NFT formation. Finally, we show that enhanced dnNT in APP/PS1 mice seems to differ from age-associated dnNT, as neurons located in deep layers of the cerebral cortex are differentially affected by these processes.

2. Material and methods

2.1. Patients and healthy controls

Samples of frontal, parietal, and EC from AD patients, and from healthy controls without any history of neurological or psychiatric illness (see Table 1) were provided by the Banco de Tejidos Fundación CIEN (BT-CIEN; Madrid, Spain) and the Banco de Cerebros de la Región de Murcia (Hospital Virgen de la Arrixaca, Murcia, Spain). Written informed consent for brain removal after death for diagnostic and research purposes was obtained from brain donors and/or next of kin. Immediately after postmortem brain extraction, each brain was sagittally divided into 2 symmetrical halves. The right brain half was subsequently cut in slices and frozen in −60 °C isopentane, whereas the left half was fixed by immersion in 4% phosphate-buffered formaldehyde. A full neuropathological examination of each brain was performed on the left brain half. Severity of Alzheimer pathology was scored according to the National Institute on Aging—Alzheimer's Association Guidelines, following the "ABC" protocol (Montine et al., 2012). Consequently total amyloid burden ("A" score) was determined according to the Thal staging system; the stage of neurofibrillary pathology was established according to the Braak ("B" score) scheme; and the frequency of neuritic plaques in associative cortex according to the Consortium to Establish a Registry for AD protocol ("C" score) was registered. Procedures have been approved by the Scientific Committee of BT-CIEN and the Bioethics Committee of Consejo Superior de Investigaciones Científicas (CSIC).

2.2. Mice

APP/PS1 double transgenic mice (Fernandez et al., 2012) were kindly provided by I. Torres-Aleman (Cajal Institute, Spain). APP/PS1 double transgenic mice were genotyped as described by Fernandez et al. (2012). Males and females were used interchangeably with no differences between genders (not shown). Original breeding pairs of mice homozygous for a null mutation of the *E2f1* gene ($E2f1^{-/-}$) (Field et al., 1996) were obtained from The Jackson Laboratory (stock number: 002785). These mice were backcrossed to the C57BL6/J genetic background for 9 generations ($E2f1^{-/-}$ in C57BL6/J genetic background [C57-$E2f1^{-/-}$] mice). C57BL6/J (wild type in C57BL6/J genetic background [C57-WT]) and C57-$E2f1^{-/-}$ mice were used in the present study. Genotypes were determined by genomic polymerase chain reaction as following the protocol provided by The Jackson Laboratory. Experimental procedures were approved by the CSIC Bioethics Committee, in accordance with the European Union guidelines.

2.3. Primary and secondary antibodies

The rat anti-CTIP2 monoclonal antibody [25B6] (Abcam) was used at 1/500 for immunohistochemistry and 1/400 for flow cytometry. The rabbit anti-MEF2C polyclonal antibody ab64644 (Abcam) was diluted 1/500 for immunohistochemistry and 1/300 for flow cytometry. The rabbit anti-Etv1 antibody (GeneTex) was used at 1/500 dilution. The rabbit anti-NeuN polyclonal antibody (Merck Millipore) was diluted 1/800 for flow cytometry, and the mouse anti-NeuN monoclonal antibody (clone A60, Merck Millipore) was used at 1/800 dilution for flow cytometry. The mouse anti-NeuN (Chemicon) was used at 1/1000 dilution for immunohistochemistry. The goat antibody against doublecortin (DCX; Santa Cruz) was diluted 1/500, and the rabbit antibody anti-calretinin (Swant) was used at 1/3000 dilution. Secondary anti-mouse or anti-rabbit antibodies, generated in donkey or goat and conjugated to Alexa Fluor 488, 594, or 647, were purchased from Invitrogen. These antibodies were used at 1/500 dilution for cytometry and 1/1000 for immunohistochemistry.

2.4. Immunohistochemistry

Brains of 2-month-old mice perfused with 4% paraformaldehyde (PFA) were postfixed for 8–12 hours at 4 °C with PFA, and cryosectioned after embedding in tissue-tek optimal cutting temperature compound (Sakura). Cryosections (20 μm) were permeabilized and blocked for 1 hour at room temperature (RT) in PBS containing 0.1% Triton X-100 (PTx) and 10% fetal calf serum (FCS; Invitrogen), and incubated over night at 4 °C with the primary antibody in PTx plus 1% FCS. After washing with PTx, the sections were incubated for 1 hour at RT in PTx plus 1% FCS with the secondary antibodies. The sections were finally washed in PTx, and incubated with 100 ng/mL 4′,6-diamidino-2-phenylindole (DAPI; Sigma) in phosphate buffered saline (PBS) before mounting. For DCX, calretinin, and NeuN detection in the mouse dentate gyrus (DG), EC, and motor cortex (MC), coronal brain sections (50 μm) were obtained through the whole hippocampus using a vibratome (VT-1000s, Leica, Bensheim, Germany). Coronal brain sections (50 μm) were pretreated for 10 minutes with PBS containing 1%

Table 1
List of cases used in this study

Case	Gender	Age (y)	Braak	Thal	NP	% 4C NeuN$^+$			% 4C MEF2C$^+$-NeuN$^+$		% 4C Etv1$^+$-NeuN$^+$	
						PCx	FCx	EntCx	PCx	FCx	PCx	FCx
BCPA0188	M	46	ND	ND	0	1.38 ± 0.27 ($n = 5$)	1.28 ± 0.23 ($n = 5$)	1.84 ± 0.41 ($n = 4$)	4.40 ± 0.72 ($n = 3$)	3.31 ± 1.21 ($n = 3$)	1.45 ± 0.63 ($n = 3$)	1.50 ± 0.06 ($n = 3$)
BCM122	M	53	0	0	0	3.25 ± 0.85 ($n = 2$)	1.83 ± 0.13 ($n = 2$)	1.78 ± 0.18 ($n = 2$)	4.35 ± 0.85 ($n = 2$)	2.70 ± 1.30 ($n = 2$)	2.85 ± 0.25 ($n = 2$)	2.05 ± 0.25 ($n = 2$)
BCM118	M	54	0	0	0	1.53 ± 0.38 ($n = 2$)	1.2 ± 0.05 ($n = 2$)	1.83 ± 0.03 ($n = 2$)	1.70 ± 0.20 ($n = 2$)	1.55 ± 0.05 ($n = 2$)	1.50 ± 0.20 ($n = 2$)	1.60 ± 0.40 ($n = 2$)
BCM0093	F	55	0	0	0	1.16 ± 0.15 ($n = 5$)	1.51± 0.16 ($n = 5$)	1.73 ± 0.12 ($n = 3$)	1.36 ± 0.33 ($n = 3$)	1.20 ± 0.30 ($n = 2$)	0.86 ± 0.32 ($n = 3$)	1.70 ± 0.50 ($n = 2$)
BCPA0177	F	58	0	2	0	1.57 ± 0.35 ($n = 5$)	1.57 ± 0.24 ($n = 5$)	2.07 ± 0.26 ($n = 3$)	4.27 ± 0.38 ($n = 3$)	2.33 ± 0.47 ($n = 3$)	2.07 ± 0.20 ($n = 3$)	1.30 ± 0.15 ($n = 3$)
BCM0098	F	62	0	0	0	1.26 ± 0.08 ($n = 5$)	1.06 ± 0.13 ($n = 2$)	2.23 ± 0.40 ($n = 5$)	2.34 ± 0.17 ($n = 3$)	1.56 ± 0.61 ($n = 3$)	1.17 ± 0.09 ($n = 3$)	1.07 ± 0.19 ($n = 3$)
BCM144	M	76	0	3	0	2.00 ± 0.10 ($n = 2$)	1.6 ± 0.05 ($n = 2$)	2.25 ± 0.10 ($n = 2$)	4.45 ± 0.15 ($n = 2$)	3.50 ± 2.30 ($n = 2$)	2.10 ± 0.50 ($n = 2$)	1.60 ± 0.00 ($n = 2$)
BCPA0056	M	75	2	5	2	2.69 ± 0.39 ($n = 5$)	2.28 ± 0.33 ($n = 5$)	ND	5.34 ± 0.18 ($n = 3$)	3.02 ± 0.90 ($n = 3$)	3.42 ± 0.64 ($n = 3$)	2.10 ± 0.51 ($n = 3$)
BCM137	M	78	2	0	0	1.28 ± 0.08 ($n = 2$)	1.3 ± 0.20 ($n = 2$)	ND	2.15 ± 0.45 ($n = 2$)	1.80 ± 0.80 ($n = 2$)	1.40 ± 0.70 ($n = 2$)	1.75 ± 0.25 ($n = 2$)
BCPA0014	M	80	2	0	0	1.92 ± 0.29 ($n = 5$)	1.88 ± 0.26 ($n = 5$)	ND	4.09 ± 1.02 ($n = 3$)	2.22 ± 0.27 ($n = 3$)	1.81 ± 0.52 ($n = 3$)	1.90 ± 0.15 ($n = 3$)
BCPA0019	F	85	2	1	0	2.17 ± 0.48 ($n = 5$)	2.16 ± 0.32 ($n = 5$)	ND	5.47 ± 0.29 ($n = 3$)	4.22 ± 1.85 ($n = 3$)	2.80 ± 0.85 ($n = 3$)	2.30 ± 0.74 ($n = 3$)
BCPA0062	F	87	2	1	0	1.77 ± 0.40 ($n = 5$)	1.96 ± 0.37 ($n = 5$)	ND	3.86 ± 0.96 ($n = 3$)	3.66 ± 0.74 ($n = 3$)	2.82 ± 0.64 ($n = 3$)	2.40 ± 0.46 ($n = 3$)
BCPA0212	M	79	4	4	2	3.12 ± 0.60 ($n = 5$)	2.83 ± 0.55 ($n = 5$)	ND	5.82 ± 1.33 ($n = 3$)	6.27 ± 1.26 ($n = 3$)	4.59 ± 1.26 ($n = 3$)	4.20 ± 1.06 ($n = 3$)
BCPA0025	M	85	3	5	1	1.95 ± 0.48 ($n = 5$)	1.96 ± 0.17 ($n = 4$)	ND	5.37 ± 0.92 ($n = 3$)	4.34 ± 0.76 ($n = 3$)	2.36 ± 0.59 ($n = 3$)	2.13 ± 0.24 ($n = 3$)
BCPA0143	M	88	4	5	2	2.29 ± 0.25 ($n = 5$)	2.76 ± 0.22 ($n = 5$)	ND	5.53 ± 0.28 ($n = 3$)	6.08 ± 0.68 ($n = 3$)	3.09 ± 0.81 ($n = 3$)	3.33 ± 0.62 ($n = 3$)
BCPA0067	F	91	4	4	2	1.93 ± 0.12 ($n = 5$)	1.85 ± 0.17 ($n = 4$)	ND	5.05 ± 0.05 ($n = 3$)	3.17 ± 0.59 ($n = 3$)	2.08 ± 0.41 ($n = 3$)	2.33 ± 0.42 ($n = 3$)
BCPA0155	M	71	6	5	3	3.48 ± 0.58 ($n = 5$)	2.9 ± 0.57 ($n = 5$)	ND	8.88 ± 0.86 ($n = 3$)	7.76 ± 0.67 ($n = 3$)	4.70 ± 1.27 ($n = 3$)	5.37 ± 1.30 ($n = 3$)
BCPA0124	F	79	6	5	3	2.81 ± 0.51 ($n = 5$)	2.48 ± 0.17 ($n = 4$)	ND	6.69 ± 0.58 ($n = 3$)	4.11 ± 0.50 ($n = 3$)	3.23 ± 1.49 ($n = 3$)	3.23 ± 0.78 ($n = 3$)
BCPA0166	M	83	6	5	3	2.92 ± 0.45 ($n = 5$)	2.76 ± 0.61 ($n = 5$)	ND	8.01 ± 1.85 ($n = 3$)	6.24 ± 1.41 ($n = 3$)	4.39 ± 1.01 ($n = 3$)	4.63 ± 1.62 ($n = 3$)
BCPA0022	M	86	5	5	2	2.35 ± 1.05 ($n = 3$)	1.7 ± 0.40 ($n = 3$)	ND	ND	ND	ND	ND
BCPA0151	F	86	6	5	3	2.19 ± 0.35 ($n = 5$)	2.65 ± 0.33 ($n = 4$)	ND	6.72 ± 0.96 ($n = 3$)	6.54 ± 0.57 ($n = 3$)	3.93 ± 0.97 ($n = 3$)	4.37 ± 0.68 ($n = 3$)
BCPA0073	F	88	5	5	3	2.33 ± 0.40 ($n = 3$)	2.92 ± 0.12 ($n = 2$)	ND	ND	ND	ND	ND

Mean ± standard error of the mean is shown.
Key: EntCx, entorhinal cortex; FCx, frontal cortex; ND, nondetermined; NP, neuritic plaque score; PCx, parietal cortex.

bovine serum albumin (BSA)/1% Triton. After being rinsed several times with PBS containing 1% BSA/1% Triton, brain sections were incubated with the primary antibody and subsequently with the corresponding secondary antibody in each case. Chromogen reactions were performed with DAB (Sigma-Aldrich) and 0.003% H_2O_2 for 3 minutes. For the immunofluorescence cell nuclei detection, all the sections were counterstained for 12 minutes with DAPI (1/1000, Calbiochem-EMD Darmstadt, Germany). Immunohistochemistry of human frontal cortex was performed in cryostat sections (4–6 μm) obtained from frozen samples. Cryosections were fixed in acetone for 5–10 minutes at 4 °C. After letting them dry for an additional 30 minutes period at RT, sections were fixed again in chloroform for 20–30 minutes and then hydrated in distilled water for 15 minutes and washed in PBS. After incubating the sections for 10 minutes at RT in 100 mM sodium borohydride (Sigma-Aldrich) in PBS, pH 7.6, they were washed with PBS. Sections were then permeabilized and blocked for 1 hour at RT in PBS containing PTx/10% FCS, and immunostained as described above. Fluorescent labeling was assessed using a TCS SP5 confocal microscope (Leica).

2.5. Cell nuclei isolation and immunostaining

Cell nuclei isolation was performed following a procedure modified from López-Sánchez and Frade (2013a). Briefly, fresh-frozen human and mouse tissues (1 mouse hemicortex or a cube of 5–8 mm edge of human brain tissue) were placed in 3.0 mL ice-cold, DNase-free PTx containing protease inhibitor cocktail (Roche). Cell nuclei were then isolated by mechanical disaggregation using a Dounce homogenizer and then diluted up to 4.5 mL with PTx. Undissociated tissue was removed by centrifugation in 1.5-mL minifuge tubes at 200 × g for 1.5 minutes at 4 °C. Supernatants were reserved, and pellets were washed with 1.5 mL PTx and centrifuged at 100 × g for 2 minutes at 4 °C. Supernatants were collected and added to the previous ones. These samples were 8-fold diluted with PTx and centrifuged at 400 × g for 4 minutes at 4 °C. Supernatants, which lacked cell nuclei (not shown; but see López-Sánchez and Frade, 2013b), were discarded, and the pellet incubated at 4 °C in 800–1000 μL cold PTx for at least 20 minutes, prior to mechanical disaggregation by gently swirl of the vial. The quality and purity of the isolated nuclei was checked microscopically after staining with 100 ng/mL DAPI.

Nuclear immunostaining was performed as previously described (López-Sánchez and Frade, 2013a, 2015). Briefly, primary and secondary antibodies were added to isolated unfixed nuclei containing 5% of FCS and 1.25 mg/mL of BSA. In control samples, the primary antibodies were excluded. Finally, the reaction was incubated over night at 4 °C in the dark. Immunostained nuclei, whose average maximum diameter in human cortex was estimated to be 9.75 ± 0.21 μm (mean ± standard error of the mean [SEM]; n = 200), were filtered through a 40-μm nylon filter, able to retain big aggregates but not nuclei. Then, the volume was adjusted to 800–1000 μL with DNase-free PTx containing 40 μg/mL PI (Sigma) and 25 μg/mL DNAse-free RNAse I (Sigma), and incubated for 30 minutes at RT. The quality of the nuclei and specificity of immunostaining signal was checked by fluorescence microscopy.

2.6. Fluorescent in situ hybridization (FACS)

Flow cytometry was carried out using a FACSAria cytometer (BD Biosciences, San Diego, CA, USA) equipped with a 488-nm Coherent Sapphire solid state and 633-nm JDS Uniphase HeNe air-cooled laser. The emission filters used were BP 530/30 for Alexa 488, BP 616/23 for propidium iodide (PI) and BP 660/20 for Alexa 647. Data were analyzed with FACSDiva (BD Biosciences) and Weasel 3.0.1 (Walter and Eliza Hall Institute of Medical Research) softwares, and displayed using biexponential scaling. Cellular debris, which was clearly differentiated from nuclei due to its inability to incorporate PI, was gated and excluded from the analysis. DNA content histograms were generated excluding doublets and clumps by gating on the DNA pulse area versus its corresponding pulse height (Nunez, 2001). For maximum doublet resolution, minimal flow rate was used in all experiments. The exclusion of doublets was confirmed by checking the DNA pulse area versus the pulse width of the selected population. The percentage of tetraploid nuclei was quantified by using the ModFit software package (Verity). A range of 20,000–40,000 positive nuclei was analyzed for each neuronal population.

2.7. Whole genome amplification (WGA) and comparative genomic hybridization (CGH) array

Genomic DNA from 1000 tetraploid NeuN-positive nuclei, obtained by FACS from the parietal cortex of control individuals, was amplified using the PicoPLEX WGA kit (New England Biolabs) following the instructions of the manufacturer. CGH arrays were performed using the SurePrint G3 Human CGH Microarray Kit 180K (Agilent Technologies) covering the whole genome with a 13 Kb overall median probe spacing (11 Kb for RefSeq genes), following the manufacturer's protocol. Bioinformatic analysis was performed using Feature Extraction and Cytogenomics softwares (Agilent Technologies).

2.8. Slide-based cytometry (SBC)

The relative DNA content present in tetraploid, NeuN-positive nuclei isolated by FACS from human parietal cortex was analyzed by SBC. To this end, nuclei were dropped onto microscope slides, and mounted in glycerol/PBS (1:1). NeuN-positive immunostaining and PI labeling was then captured under linear conditions with a 40× magnification objective using a Nikon E80i microscope equipped with a DXM 1200 digital camera (Nikon, Melville, NY, USA). The integral density of PI, obtained as arbitrary units, was quantified using the freely available ImageJ software (National Institute of Health, Bethesda, Maryland, USA). Average intensity of each nuclei present in doublets was used to define the integral density of diploid DNA content.

2.9. Fluorescence in situ hybridization (FISH)

FISH was performed using a modification of a previously described protocol (Chaumeil et al., 2013). Isolated cell nuclei from human parietal cortex were immunolabeled with anti-NeuN antibodies as described for FACS. Cell nuclei were then dropped onto microscope slides, fixed with 2% PFA for 10 minutes at RT, rinsed in PBS and permeabilized for 10 minutes on ice in PBS containing 0.7% Triton X100. FISH was performed using an XCE 8 XCyting Centromere Enumeration Probe (MetaSystems), which recognizes the centromeric region of human chromosome 8, following the indications of the manufacturer with minor modifications (30 minutes denaturation time). Nuclei were finally mounted with ProLong Diamond Antifade Mountant with DAPI (Molecular Probes) and microscopically analyzed as describe above.

2.10. Behavioral tests

2.10.1. Morris water maze (MWM) test

The water maze test was adapted from Morris (1981). The MWM test apparatus consisted of a circular methacrylate tank (100 cm in diameter). The pool was filled with 120 L water at RT (21 °C–22 °C).

The pool was divided into 4 virtual quadrants (Q1, Q2, Q3, and Q4) of equal surface area. A transparent escape methacrylate platform (8 cm in diameter, 18 cm in height) was placed in a fixed location in the tank, 1 cm below the water surface. Many cues surrounded the maze and were available for the mice to use in locating the escape platform. During training trials, the platform remained in a constant location in the center of one quadrant. After habituating each mouse to the maze in the absence of platform, they received either 2 (demanding conditions) or 4 (standard conditions) trials per day for 4 days. Each training trial involved placing the mouse into the pool facing the wall at one of the 4 quadrants. A different starting point was randomly used on each trial. The mice were allowed to swim freely until they found the escape platform. The latency to find the hidden platform was recorded and used as a measure of acquisition of the task. If a mouse failed to locate the platform within 60 seconds it was then manually guided to the escape platform by the experimenter and allowed to stay 20 seconds on the platform. Twenty-four hours after the last training trial, the platform was removed from the pool, the mice were allowed to swim for 90 seconds in the pool and the time spent in the target quadrant (the quadrant in which the platform was during training) was recorded. The percentage of time spent in the target quadrant was used as an index of memory acquisition. This same test was repeated 10 days after the last training trial, and the time spent in the target quadrant was recorded. The percentage of time spent in the target quadrant was used as an index of memory consolidation.

2.10.2. Novel object recognition (NOR) test

The NOR test was adapted from Ennaceur and Delacour (1988). In the object recognition protocol, 2 different objects were placed in the arena during the training phase. After a delay of 1 or 24 hours, one object was changed to a novel object. The aim was to test the local mouse's memory of the original objects by measuring the amount of time spent exploring the novel object versus the familiar one. Selected objects consisted of plastic pieces with different forms and were thoroughly cleansed between trials to ensure the absence of olfactory cues (Fontán-Lozano et al., 2007). Each mouse was first placed in the open box (30 × 40 × 30 cm) made of laminated agglomerate with the inside painted nonreflecting gray, and exposed for either 5 minutes (demanding conditions) or 15 minutes (standard conditions) to 2 objects (A, B) placed approximately 10 cm distant from 2 adjacent corners of the box. The mouse was then returned to its home cage. After a delay of 1 hour the mouse was presented with one of the familiar objects (A) and a novel object (C) for a further 5 minutes (demanding conditions) or 15 minutes (standard conditions). Then, the mouse was returned again to its home cage. After a delay of 1 day the mouse was presented with one of the familiar objects (A) and a novel object (D) for a further 5 minutes (demanding conditions) or 15 minutes (standard conditions). As far as could be ascertained, the objects had no natural significance for the mice and they had never been associated with a reinforcer. Care was taken to avoid olfactory stimuli by cleaning the objects carefully with ethanol. The time spent exploring the objects (A and B, A and C, and A and D) was recorded using EthoVision XT software (version 5) and analyzed using EthoVision XT software (version 7). The relative exploration of the novel object was expressed by a discrimination index $[DI = (t_{novel} - t_{familiar})/(t_{novel} + t_{familiar})]$. The criteria for exploration were based strictly on active exploration, during which the mouse had both forelimbs within a circle of 1.5 cm around the object, with its head oriented toward it, or was touching it with its vibrissae.

2.10.3. Rotarod test

Motor coordination was evaluated in a rotarod apparatus (Ugo Basile, Italy) with increasing acceleration. The apparatus consisted of a horizontal motor-driven rotating rod in which the animals were placed perpendicular to the long axis of the rod, with the head directed against the direction of rotation so that the mouse has to progress forward to avoid falling. The trial was stopped when the animal fell down or after a maximum of 5 minutes. The time spent in the rotating rod was recorded for each animal and trial. Animals received a pretraining session to familiarize them with the procedure before evaluation. Thereafter, a total of 6 consecutive trials were done for every animal. Data are presented as the average time spent before falling from the apparatus and average number of falls in the 6 trials.

2.10.4. Activity cage test

Exploratory locomotor activity was recorded using a Hamilton–Kinder Photobeam System in an open field (40 cm × 40 cm) over a 10 minutes period. Infrared beams automatically record horizontal movements and rearing in the open field. The task analyzes the activity behavior by measuring the number of beams that are broken during the designated period of time. Ten trials repeated in 2 consecutive days (5 trials/day) were performed for every animal and results were expressed as average number of broken beams per trial.

2.10.5. Elevated plus maze (EPM) test

Each mouse was subjected to a single 5 minutes trial in the EPM test (Cibertec, Madrid, Spain), which consisted of 2 closed arms (5 cm wide × 30 cm long, with clear perplex walls 15 cm high), and 2 open arms (5 cm × 30 cm) raised 40 cm from the floor. During each trial, the mice were placed in the center of the maze and allowed to move freely along the apparatus under a constant intense white light. The movement of the animals was recorded and analyzed using Noldus EthoVision software and the data are presented as the total time (seconds) spent standing or walking in the closed arms, in the open arms, or in the hub.

2.11. Stereological analysis

The DCX, DCX/calretinin, or NeuN labeled cells were counted in the series of vibratome sections under an optical fluorescence microscope (Leica DMI 6000 B, oil immersion 40× objective), using the optical fractionator method, and the number of cells counted was multiplied by 8 to obtain the total number of cells. The total number of immature (DCX) and mature granule neurons was calculated using the physical-dissector method adapted for confocal microscopy (Leica TCS SP5) (Llorens-Martín et al., 2006). A randomly chosen series was Nissl stained to calculate the subgranular zone area of each mouse's DG using the Cavalieri method and Neurolucida software (MBF Bioscience).

2.12. Statistical analysis

For mouse samples, the percentage of tetraploidy in each experimental point was referred to the level of tetraploidy in control samples of cerebral cortex of 2-month-old, WT mice. All experiments were analyzed using at least 4 mice for each genotype/age, and repeated at least 3 times in order to calculate the average values for each experimental point (mean ± SEM). For human samples, quantification of the percentage of tetraploidy for each individual was repeated 2–5 times (NeuN analysis) and 2–3 times (neuronal subpopulation analysis), depending on the availability of the samples (see Table 1). Average values for each individual were used to calculate the mean ± SEM for each experimental point. Statistical differences were analyzed using unpaired Student's *t*-test. For behavioral analysis, 2-way ANOVA was used to make intergroup and intragroup comparisons, and post hoc analysis was made with respect to the initial habituation.

3. Results

3.1. Age-associated dnNT in WT mice occurs in neurons located in superficial and deep cortical layers

By using a highly sensitive and quantitative procedure based on flow cytometry with fresh cell nuclei, we have previously shown that a small proportion of differentiating projection neurons become tetraploid during the development of the mouse cerebral cortex (López-Sánchez and Frade, 2013a, 2015), an observation that was confirmed by FISH (López-Sánchez and Frade, 2013a). To explore whether tetraploidization of fully differentiated neurons also occurs in the normal adult brain, we performed flow cytometry in isolated cell nuclei from mouse cerebral cortex (see Fig. S1 for singlet gating procedures, and Figs. 1A–D, 2A–F, and 3A–D for tetraploid neuron detection). This analysis demonstrated a statistically significant increase ($p = 3.09 \times 10^{-9}$) in the proportion of tetraploid cortical neurons, revealed with the well-characterized neuronal marker NeuN (Mullen et al., 1992; Wolf et al., 1996), when 5-month-old mice were compared with mice of 2 months of age (Fig. 1E).

To define the neuronal phenotypes that become tetraploid in the adult cerebral cortex we focused on MEF2C, a transcription factor known to be expressed by cells located in the superficial cortical layers (Leifer et al., 1993), and CTIP2, a transcription factor expressed by subcortical projection neurons located in layer V–VI (Arlotta et al., 2005). These markers were chosen as they localize to the nuclear compartment, thus allowing the analysis of cell nuclei by flow cytometry. Although at perinatal stages MEF2C identifies cells located in the superficial cortical layers (Leifer et al., 1993), our immunohistochemical analyses indicated that, in the adult cerebral cortex, MEF2C can also be detected at low levels in cells situated in the deep layers (Fig. S2A in Supplementary Material). Nevertheless, neurons expressing high levels of MEF2C (i.e., neurons located superficially), were easily distinguished by flow cytometry. This technique evidenced 2 main neuronal populations (revealed by the expression of the neuronal marker NeuN), one showing high levels of MEF2C and another one expressing low levels of this transcription factor (Fig. S2B in Supplementary Material). Double labeling with MEF2C and CTIP2 antibodies revealed that the former population lacks CTIP2 expression (Fig. S2C in Supplementary Material), thus confirming that the NeuN-positive population showing intense MEF2C labeling contains superficially-located neurons. By using high intensity MEF2C/NeuN and CTIP2 as markers, we found that age-associated tetraploidization equally affects to neurons from both superficial ($p = 0.020$) (Fig. 2G) and deep ($p = 0.017$) (Fig. 3E) cortical layers.

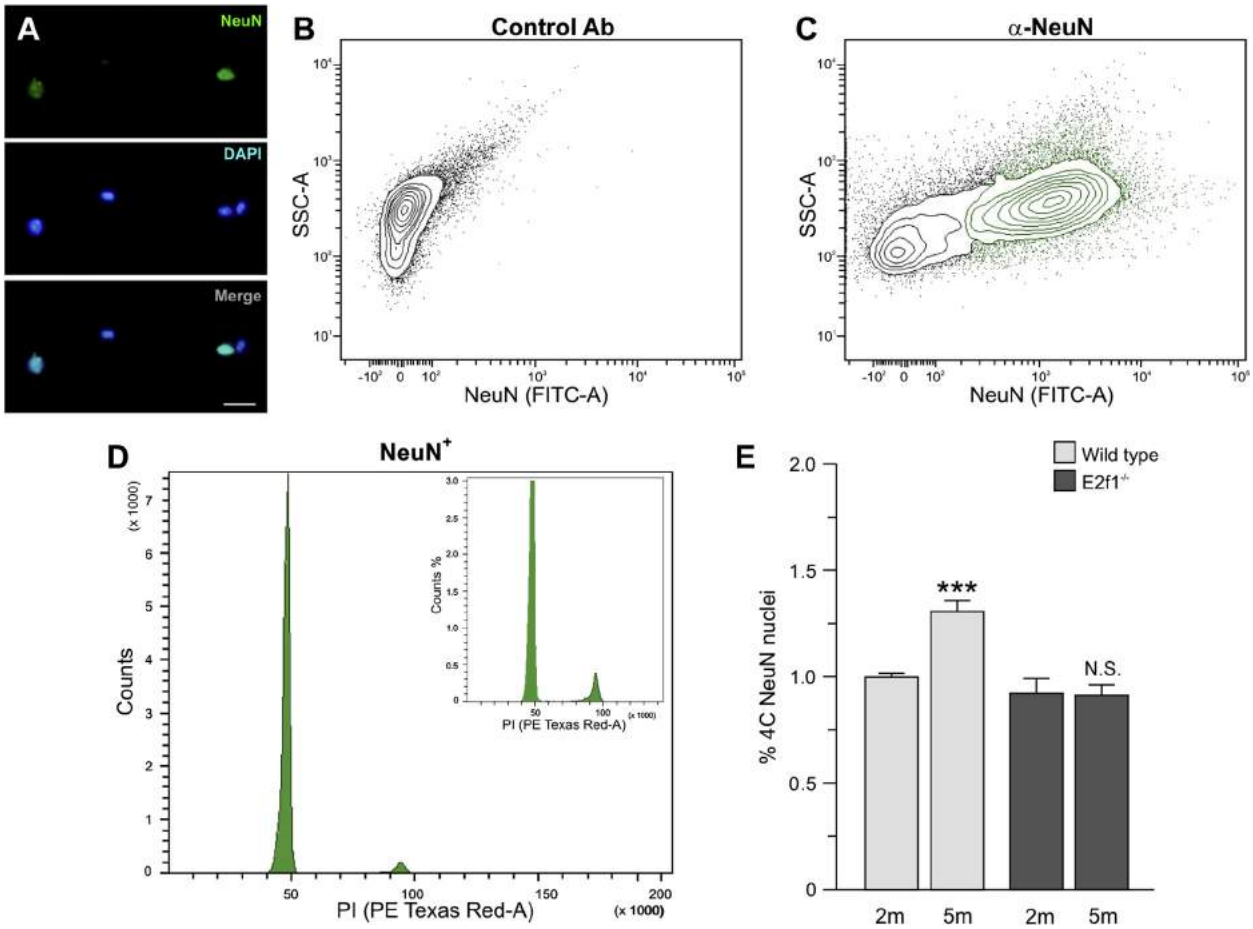

Fig. 1. dnNT affects the mouse cerebral cortex and is prevented in C57-*E2f1*$^{-/-}$ mice. Fresh cell nuclei preparations from cerebral cortex of C57-WT and C57-*E2f1*$^{-/-}$ mice of either 2 or 5 months of age were immunostained with an anti-NeuN specific antibody. (A) Cortical cell nuclei immunostained with anti-NeuN and counterstained with DAPI. Bar: 20 μm. Cortical cell nuclei immunostained with anti-NeuN (C) or with the secondary antibody alone (B) were PI stained and subjected to flow cytometric analysis. NeuN-positive nuclei are shown in green. (D) Representative histogram illustrating DNA content in NeuN-positive nuclei, as evaluated by PI labeling (PE-Texas Red-A). Insert shows a magnification of the histogram. (E) The percentage of tetraploid neurons (% 4C NeuN-positive nuclei) was significantly increased in the cerebral cortex of 5-month-old C57-WT mice (wild type), but not of C57-*E2f1*$^{-/-}$ mice (E2f1$^{-/-}$). $^{***}p < 0.005$. Abbreviations: C57-E2f1$^{-/-}$, E2f1$^{-/-}$ in C57BL6/J genetic background; C57-WT, wild type in C57BL6/J genetic background; DAPI, 4′,6-diamidino-2-phenylindole; dnNT, de novo-generated neuronal tetraploidy; N.S., nonsignificant; PI, propidium iodide. (For interpretation of the references to color in this figure legend, the reader is referred to the Web version of this article.)

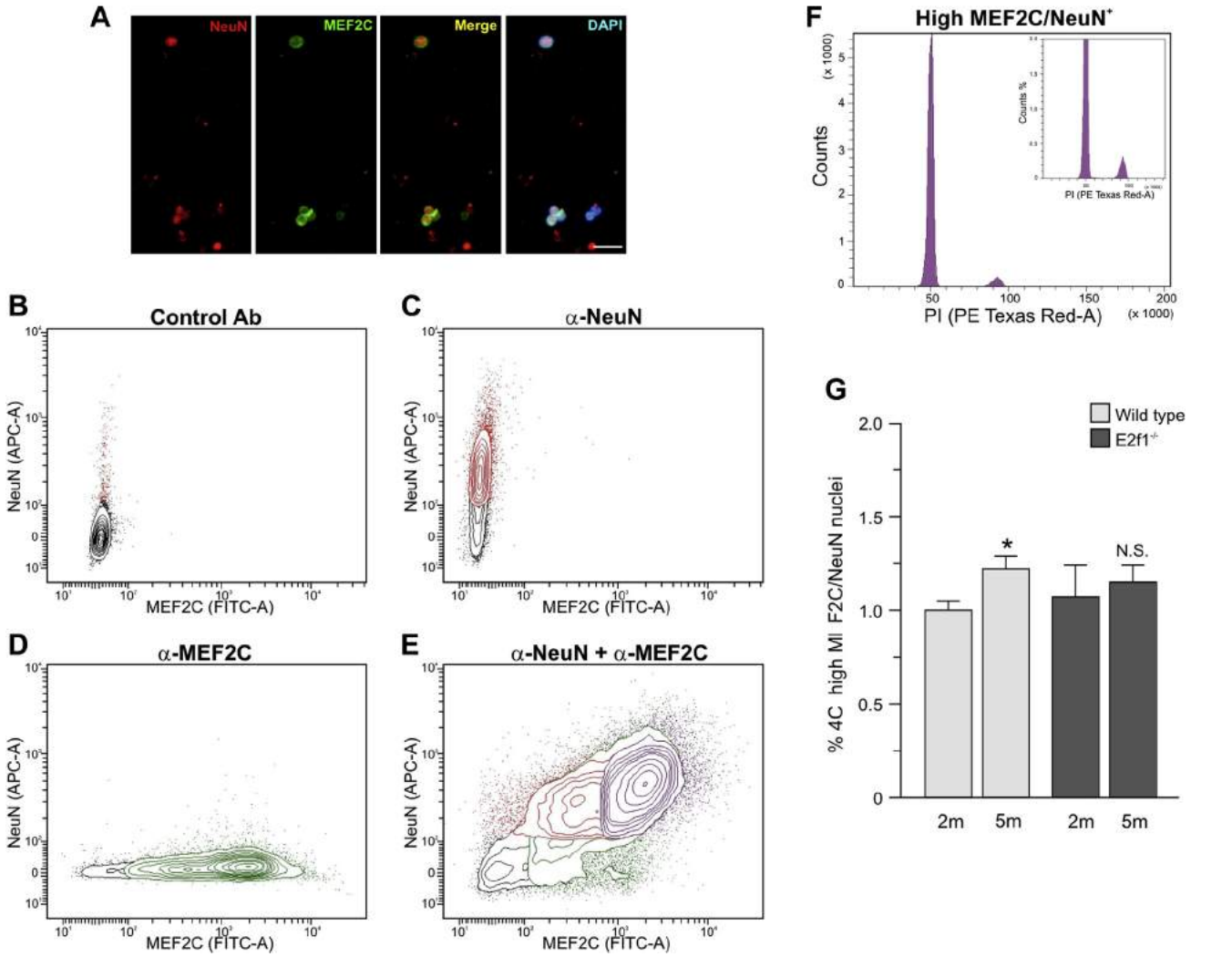

Fig. 2. dnNT takes place in the superficial layers of the mouse cerebral cortex and is prevented in C57-*E2f1*$^{-/-}$ mice. Fresh cell nuclei preparations from cerebral cortex of C57-WT and C57-*E2f1*$^{-/-}$ mice of either 2 or 5 months of age were immunostained with anti-NeuN plus anti-MEF2C specific antibodies to identify neurons located in the superficial layers. (A) Cortical cell nuclei immunostained with anti-NeuN and anti-MEF2C and counterstained with DAPI. Bar: 20 μm. Cortical cell nuclei immunostained with anti-NeuN (C), anti-MEF2C (D), both antibodies (E), or secondary antibody alone (B) were PI stained and subjected to flow cytometric analysis. MEF2C-positive nuclei lacking NeuN are shown in green, NeuN/low MEF2C-positive nuclei are shown in red, and NeuN/high MEF2C-positive nuclei are shown in purple. (F) Representative histogram illustrating DNA content, as evaluated by PI labeling (PE-Texas Red-A), in NeuN-positive nuclei showing high MEF2C labeling (see Fig. S2). Insert shows a magnification of the histogram. (G) The percentage of tetraploid neurons located in the superficial layers (% 4C high MEF2C/NeuN-positive nuclei) was significantly increased in the cerebral cortex of 5-month-old C57-WT mice (wild type), but not of C57-*E2f1*$^{-/-}$ mice (E2f1$^{-/-}$). $^{*}p < 0.05$. Abbreviations: C57-E2f1$^{-/-}$, E2f1$^{-/-}$ in C57BL6/J genetic background; C57-WT, wild type in C57BL6/J genetic background; DAPI, 4′,6-diamidino-2-phenylindole; dnNT, de novo-generated neuronal tetraploidy; N.S., nonsignificant; PI, propidium iodide. (For interpretation of the references to color in this figure legend, the reader is referred to the Web version of this article.)

3.2. Age-associated dnNT in the cerebral cortex of WT mice relies on E2F1

E2F1 is expressed by neurons becoming tetraploid during development (Morillo et al., 2010), and this transcription factor can be detected in neurons from the adult cerebral cortex (Fig. S3 in Supplementary Material). Therefore, we explored whether dnNT can be regulated by E2F1 in the cerebral cortex of WT mice. Flow cytometric analyses indicated that the increase of cortical neurons (i.e., NeuN-positive nuclei) with double amount of DNA observed in 5-month-old C57-WT mice is completely blocked ($p = 0.695$) in C57-*E2f1*$^{-/-}$ mice (Fig. 1E). As expected, no changes were observed in the proportion of either superficial (high intensity MEF2C/NeuN-positive) (Fig. 2G) or deep (CTIP2-positive) (Fig. 3E) layer neurons ($p = 0.546$ and $p = 0.474$, respectively) when cell nuclei from 5-month-old C57-*E2f1*$^{-/-}$ mice were compared with cell nuclei from C57-*E2f1*$^{-/-}$ mice of 2 months of age. Overall, these results demonstrate that E2F1 is required for age-associated dnNT.

3.3. dnNT blockade correlates with improved memory acquisition and consolidation

The absence of E2F1 correlated with increased cognitive function in both 5-month-old (Fig. 4A) and 1-year-old (Fig. 4B) C57-*E2f1*$^{-/-}$ mice, as evaluated by the NOR test performed under demanding conditions (5 minutes training). During the training trials, no statistically significant differences ($p = 0.254$, 5 months; $p = 0.234$, 1 year) were observed between C57-WT and C57-*E2f1*$^{-/-}$ mice with regard to the time spent in exploring the 2 different objects (Fig. 4A and B; “training phase”), thus indicating that individual mice had no preference for a specific object or place. After a delay interval of 1 hour, C57-*E2f1*$^{-/-}$ mice spent significantly more

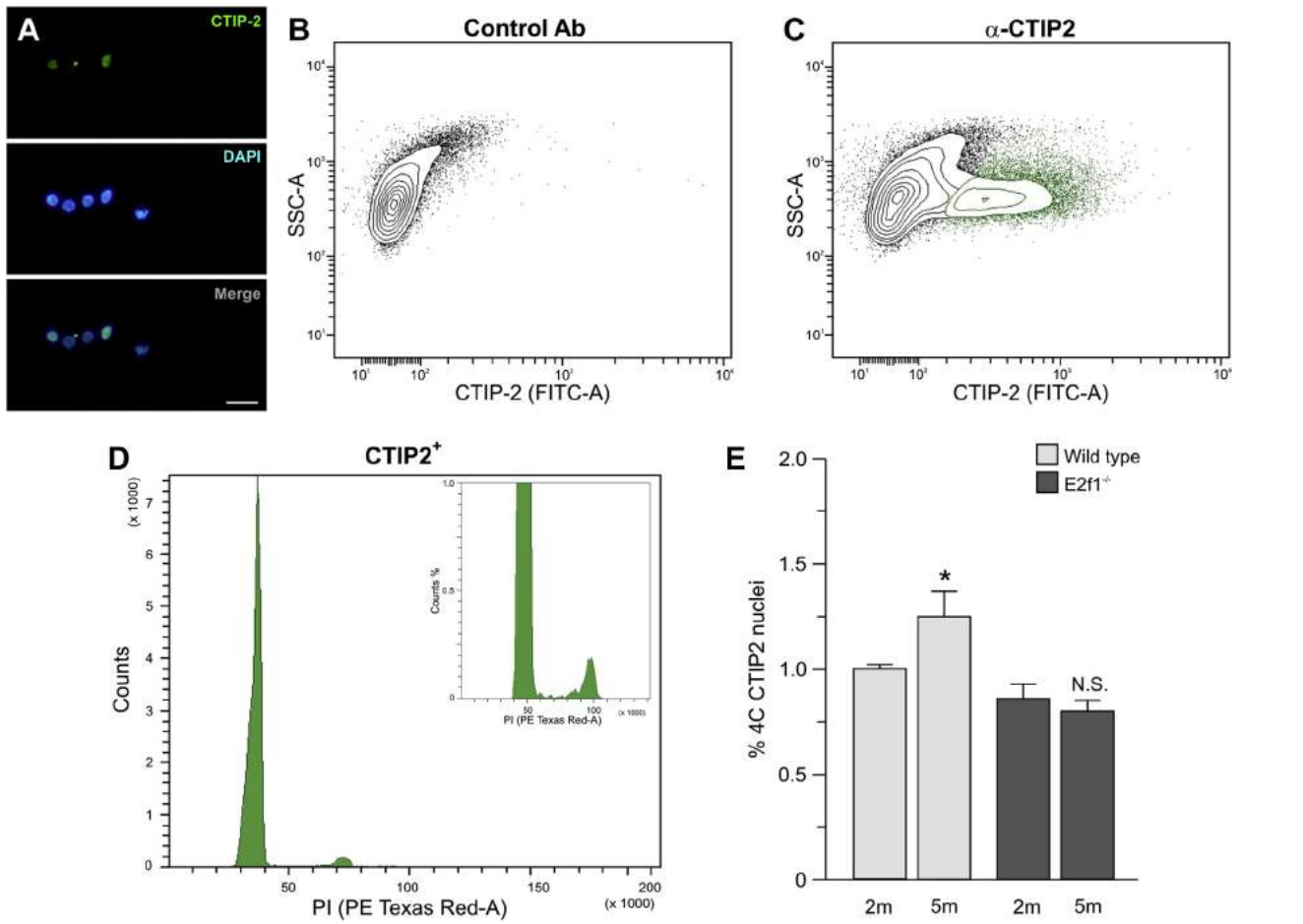

Fig. 3. dnNT takes place in the deep cortical layers of the mouse cerebral cortex and is prevented in C57-*E2f1*$^{-/-}$ mice. Fresh cell nuclei preparations from cerebral cortex of C57-WT and C57-*E2f1*$^{-/-}$ mice of either 2 or 5 months of age were immunostained with an anti-CTIP2 antibody to reveal projection neurons situated at layers V–VI. (A) Cortical cell nuclei immunostained with anti-CTIP2 and counterstained with DAPI. Bar: 20 μm. Cortical cell nuclei immunostained with anti-CTIP2 (C) or with the secondary antibody alone (B) were PI stained and subjected to flow cytometric analysis. CTIP2-positive nuclei are shown in green. (D) Representative histogram illustrating DNA content in CTIP2-positive nuclei, as evaluated by PI labeling (PE-Texas Red-A). Insert shows a magnification of the histogram. (E) The percentage of tetraploid neurons located in the deep layers (% 4C CTIP2-positive nuclei) was significantly increased in the cerebral cortex of 5-month-old C57-WT mice (Wild type), but not of C57-*E2f1*$^{-/-}$ mice (E2f1$^{-/-}$). $^{*}p < 0.05$. Abbreviations: C57-E2f1$^{-/-}$, E2f1$^{-/-}$ in C57BL6/J genetic background; C57-WT, wild type in C57BL6/J genetic background; DAPI, 4′,6-diamidino-2-phenylindole; dnNT, de novo-generated neuronal tetraploidy; N.S., nonsignificant; PI, propidium iodide. (For interpretation of the references to color in this figure legend, the reader is referred to the Web version of this article.)

time exploring the novel object than control mice, indicating that, in contrast with the latter, C57-*E2f1*-deficient mice recognized the familiar object despite the short duration of the training period. The discrimination ratio was significantly higher than chance performance ($p = 0.006$, 5 months; $p = 1.9 \times 10^{-4}$, 1 year) (Fig. 4A and B; "short-term memory"). After a 24 hours interval, C57-*E2f1*$^{-/-}$ mice still discriminated between the familiar and the novel object, being the discrimination ratio significantly higher than chance performance ($p = 0.001$, 5 months; $p = 0.003$, 1 year) (Fig. 4A and B; "long-term memory"). As a control, mice subjected to standard training conditions (15 minutes training) were able to discriminate (range of p values: $0.390–1.0 \times 10^{-6}$ at 5 months, and $3.9 \times 10^{-4}–8.0 \times 10^{-5}$ at 1 year) between the familiar and the novel object regardless of the phenotype (Fig. S4A and B in Supplementary Material).

The absence of E2F1 also correlated with better cognitive function as evaluated by the MWM test performed under demanding conditions (Fig. 4C–F). In this test, performances are dependent on the number of training sessions per day and the total training days. In a probe trial without platform, 24 hours after 2 training sessions per day (4 training days in total) (Fig. S5A and B in Supplementary Material), both 5-month-old (Fig. 4C) and 1-year-old (Fig. 4D) C57-*E2f1*$^{-/-}$ mice spent significantly more than 25% of their time (chance performance) in the quadrant that contained the platform during the training sessions ($p = 0.1 \times 10^{-6}$, 5 months; $p = 7.7 \times 10^{-5}$, 1 year), indicating that they have learned the location of the platform in this quadrant. In contrast, control mice performed significantly worse than C57-*E2f1*$^{-/-}$ mice at 5 months of age ($p = 0.003$) (Fig. 4C). When the probe trial was carried out 10 days after 2 training sessions per day (4 training days in total), both C57-*E2f1*$^{-/-}$ and control (C57-WT) mice of 5 months spent significantly more than 25% of their time in the quadrant that contained the platform during the training sessions ($p = 0.005$, control; $p = 0.1 \times 10^{-6}$, C57-*E2f1*$^{-/-}$), and C57-*E2f1*$^{-/-}$ mice showed a nonsignificant tendency ($p = 0.051$) to perform better than control mice (Fig. 4E). This latter effect was much more evident at 1 year of age, in which only C57-*E2f1*$^{-/-}$ mice were able to significantly remember the position of the quadrant that contained the platform ($p = 0.001$) (Fig. 4F). As a control, both path length and swimming speed were similar for all groups (range of $p = 0.925–0.106$, 5 months; 0.880–0.058, 1 year) in every trial except for path length at the 24 hours time point ($p = 0.008$) (Fig. S5E–H in Supplementary Material). As expected, MWM tests performed under standard

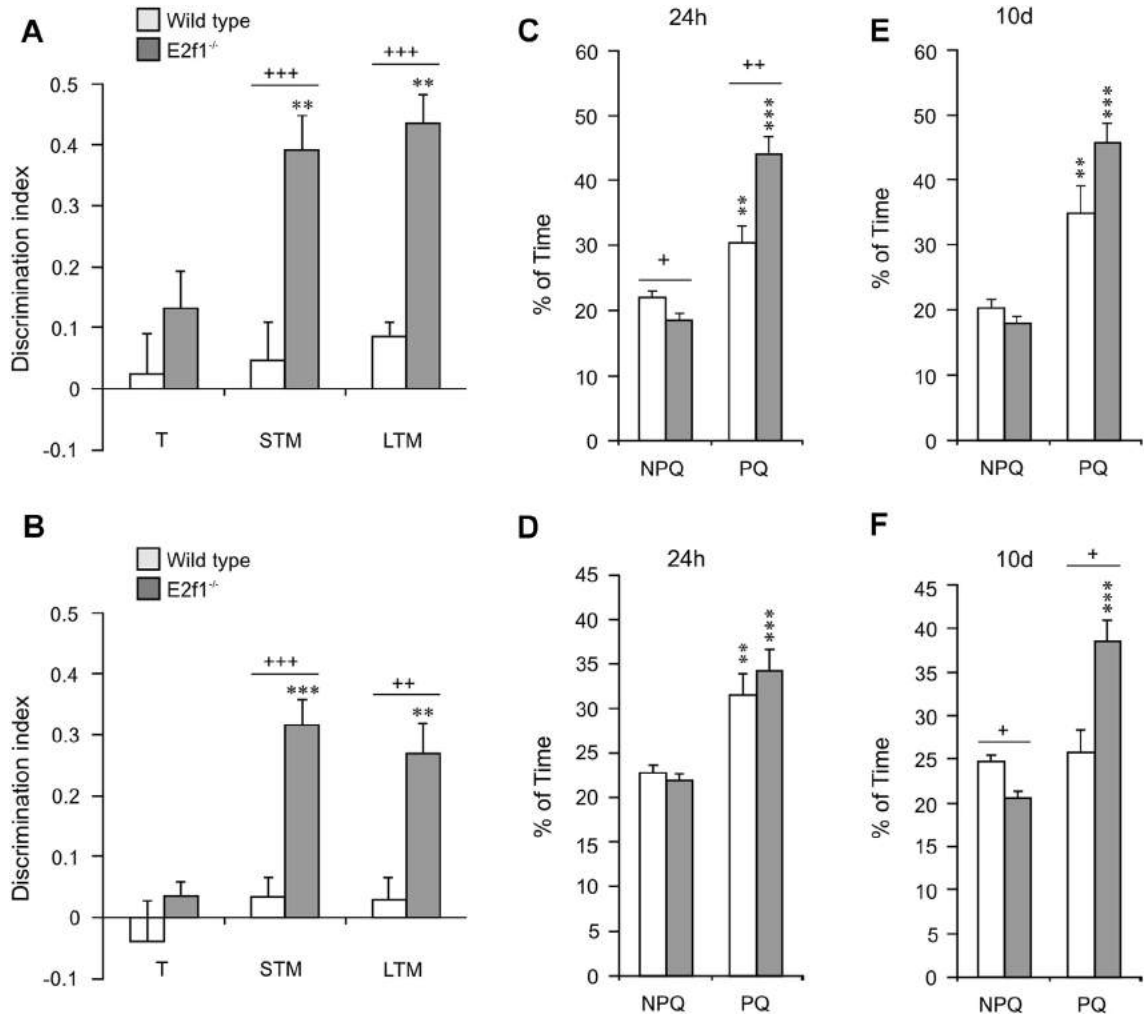

Fig. 4. Behavioral phenotyping of C57-*E2f1*$^{-/-}$ mice showing enhanced memory acquisition and consolidation compared to C57-WT controls. Novel object recognition (A, B) and Morris water maze (C–F) was assessed in both 5 months old (A, C, E) and 1-year old (B, D, F) C57-*E2f1*$^{-/-}$ (E2f1$^{-/-}$) or C57-WT (wild type) mice. When mice were analyzed in the novel object recognition test by using a demanding protocol with stringent conditions (5 minutes objects presentation), only C57-*E2f1*$^{-/-}$ mice were able to explore the novel object for longer times than the known object, both after 1 hour (STM) and 24 hours (LTM) from initial presentation, and both 5-month (A) and 1-year old (B) mice. A similar situation was found with the Morris water maze test. In a demanding protocol with stringent conditions (2 trials a day) which was sufficient for the mice to learn the task, 5-month old C57-*E2f1*$^{-/-}$ mice performed better than control mice at swimming around the learned location of the platform at a probe test, both 24 hours (C) and 10 days (E) after the last acquisition trial, while 1-year old C57-*E2f1*$^{-/-}$ mice scored better only 10 days after the last acquisition trial (compare D to F). + is used to label significant differences between genotypes; * is used to label significant differences in the comparisons to habituation training (novel object) or to the quadrants without platform (water maze); $^{+}p < 0.05$; $^{++}p < 0.01$; $^{+++}p < 0.005$; $^{**}p < 0.01$; $^{***}p < 0.005$. Abbreviations: C57-E2f1$^{-/-}$, E2f1$^{-/-}$ in C57BL6/J genetic background; C57-WT, wild type in C57BL6/J genetic background; LTM, long-term memory; NPQ, nonplatform quadrant; PQ, platform quadrant; STM, short-term memory; T, training phase.

conditions (4 training session per day along 4 days) accelerated the learning process (range of $p = 0.09–2.0 \times 10^{-5}$ 1 day after habituation), and yielded similar results for both C57-*E2f1*$^{-/-}$ and control C57-WT mice (Fig. S5C and D in Supplementary Material).

The improved performance of C57-*E2f1*$^{-/-}$ mice in both types of tests does not rely on better motor coordination as measured by a rotarod test (Fig. S6A and B in Supplementary Material) and/or locomotor activity as evidenced by an activity cage test (Fig. S6C and D in Supplementary Material) ($p = 0.904$, time on rotarod; 0.954, falls). In addition, C57-*E2f1*$^{-/-}$ mice show a statistically significant increase of anxiety as measured by an EPM test (time at the open arms: $p = 7.0 \times 10^{-4}$, 5-month-old mice; $p = 7.6 \times 10^{-4}$ 1-year-old mice) (Fig. S6E and F in Supplementary Material), a situation that theoretically would reduce their capacity to perform both behavioral tests with success.

The cognitive improvement in C57-*E2f1*$^{-/-}$ mice occurs even though compromised adult neurogenesis is detected in these mice (Cooper-Kuhn et al., 2002; Ting et al., 2014). Our results confirm that adult neurogenesis is affected in the C57-*E2f1*$^{-/-}$ mice, evidenced by the reduction in the proportion of DCX-positive cells in the DG at both 5 months ($p = 0.014$) (Fig. S7A in Supplementary Material) and 1 year ($p = 0.043$) (Fig. S7B in Supplementary Material) of age. The reduction in the proportion of DCX-positive cells in the DG mainly affects to inmature granule cells, as revealed by the expression of calretinin (Brandt et al., 2003) ($p = 0.014$, 5 months; 0.021, 1 year) (Fig. S7C and D in Supplementary Material). This indicates that the maturation of the newborn neurons is impaired in C57-*E2f1*$^{-/-}$ mice. Moreover, in agreement with the reduced apoptosis observed in the DG of C57-*E2f1*$^{-/-}$ mice (Cooper-Kuhn et al., 2002), we found a statistically significant increase ($p = 0.034$) with age of granule neurons in the DG of C57-*E2f1*$^{-/-}$ mice (Fig. S7F in Supplementary Material), whereas the amount of granule neurons show a tendency to become decreased with age in C57-WT mice (compare Fig. S7E with

Fig. S7F in Supplementary Material), likely due to enhanced apoptosis in C57-WT neurons (Cooper-Kuhn et al., 2002).

The cognitive improvement observed in C57-*E2f1*$^{-/-}$ mice occurs without substantial alterations in the number of either motor ($p = 0.208$) or entorhinal ($p = 0.157$) neurons in 1-year old C57-*E2f1*$^{-/-}$ mice (Fig. S7I and J in Supplementary Material), in agreement with the conclusions of Cooper-Kuhn et al. (2002). This was also the case for the MC of C57-*E2f1*$^{-/-}$ mice of 5 months of age ($p = 0.327$) (Fig. S7H in Supplementary Material), supporting the conclusions of Cooper-Kuhn et al. (2002). In contrast, a small, although statistically significant increase of neuronal numbers ($p = 0.043$), could be detected in the EC of 5-month-old C57-*E2f1*$^{-/-}$ mice (Fig. S7G in Supplementary Material).

Altogether, all these results indicate that memory acquisition and consolidation is improved in C57-*E2f1*$^{-/-}$ mice, in correlation with dnNT blockage.

3.4. The human cortex contains tetraploid neurons

Earlier studies have shown that the normal human cerebral cortex contains tetraploid neurons (Mosch et al., 2007). In contrast, Westra et al. (2009) were not able to detect tetraploid neurons in this structure, while these authors have reported the existence of DNA content variation in a variable proportion of cortical neurons (Westra et al., 2010). We therefore reevaluated this issue using our optimized cytometric protocol applied to the frontal and parietal cortex of normal adult individuals (see Fig. S8 in Supplementary Material for singlet gating procedures, and Fig. S9 in Supplementary Material for tetraploid neuron detection). This analysis indicated that around 1.5% of NeuN-positive nuclei show duplicated amount of DNA (Fig. 5A and B).

As expected, cell nuclei identified as tetraploid were mainly singlets with double amount of DNA. This was evidenced after isolating virtually pure diploid and tetraploid nuclear populations from the parietal cortex using 2 rounds of cell sorting (Fig. S10A and B in Supplementary Material). These nuclei were analyzed through slide-based cytometry (Fig. S11 in Supplementary Material). This analysis indicated that most cell nuclei expressed NeuN, and that tetraploid cell nuclei showed double PI intensity as compared to diploid cell nuclei (88,263 ± 4978 [$n = 16$] vs. 44,587 ± 4152 [$n = 5$], respectively; mean ± SEM, arbitrary units). Importantly, a minority of events present in the tetraploid cell nuclei preparations (12.5%) were observed to be doublets of diploid cell nuclei (PI intensity in each individual cell nuclei: 40,410 ± 5452 [$n = 6$]; mean ± SEM, arbitrary units). These latter events likely represent those located outside from the gate used for sorting (arrow in Fig. S10B in Supplementary Material), which derive from mistakes inherent to the sorting process.

We confirmed the existence of tetraploid neurons in the human cortex by performing a combination of NeuN immunofluorescence and FISH (Chaumeil et al., 2013) on PFA-preserved cell nuclei isolated from the parietal cortex. This analysis demonstrated that NeuN-positive nuclei with double amount of DNA showed 4 FISH spots whereas NeuN-positive diploid nuclei contained 2 FISH spots (Fig. 6 and Fig. S12).

3.5. Tetraploid neurons in the normal human cortex contain fully replicated genomes

To verify that DNA replication is complete and homogeneous in human tetraploid neurons, we isolated the DNA from the diploid and tetraploid nuclear populations obtained from the parietal cortex (see previous section). The genomic DNAs thus obtained were subjected to WGA, followed by CGH array experiments. This analysis demonstrated that human tetraploid neurons have completely and homogeneously replicated their DNA (Fig. S10C in Supplementary Material). Therefore, these neurons represent a cellular population that differs from that with partial DNA content described by Westra et al. (2010).

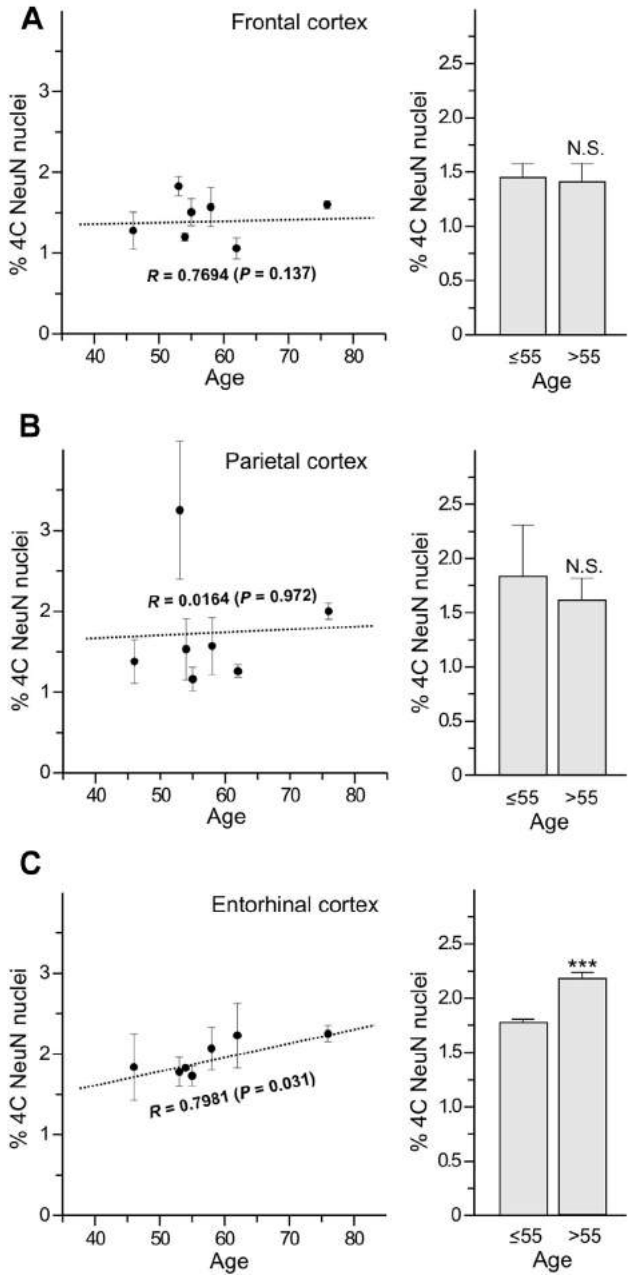

Fig. 5. The human EC show age-dependent dnNT. Fresh cell nuclei preparations from frontal (A), parietal (B), or entorhinal (C) cortices of individuals of the indicated ages were immunostained with anti-NeuN to define the whole neuronal population, labeled with PI, and subjected to flow cytometric analysis. The percentage of tetraploid neurons (% 4C NeuN nuclei) both in the frontal and in the parietal cortex was similar at the different ages that were studied (left panels in A, B). No statistically significant differences were observed when individuals were split according to their age into 2 groups of either below or above 55 years (right panels in A, B). In the EC, a statistically significant positive correlation was observed between the percentage of tetraploid neurons (% 4C NeuN nuclei) and the studied ages (left panel in C). Statistically significant differences were observed when results were split according to the age of the individual into 2 groups of either below or above 55 years (right panel). $^{***}p < 0.005$. Abbreviations: dnNT, de novo-generated neuronal tetraploidy; EC, entorhinal cortex; N.S., nonsignificant; PI, propidium iodide.

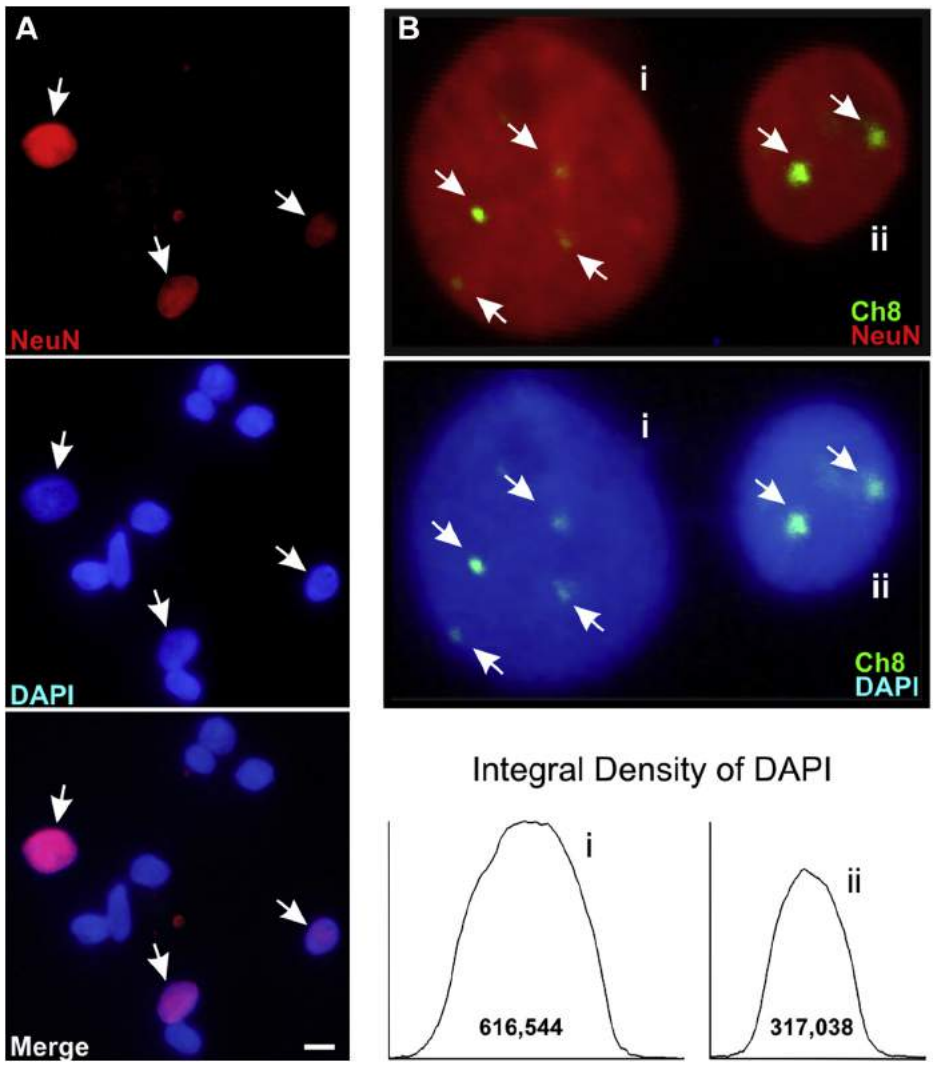

Fig. 6. Tetraploid neurons revealed by FISH. (A) Cell nuclei from the human parietal cortex, fixed with 2% PFA and immunolabeled with anti-NeuN antibodies, maintain the NeuN specific labeling (arrows) after being subjected to FISH conditions. (B) NeuN-positive cell nuclei from the human parietal cortex subjected to FISH with a chromosome 8-specific probe (Ch8) and counterstained with DAPI. (i) tetraploid neuron with 4 FISH spots; and (ii) diploid neuron with 2 FISH spots. Bottom panel: distribution of DAPI density and DAPI integral density values in arbitrary units (i.e., DNA content) of the illustrated neuronal nuclei, quantified by ImageJ software. Bar: 20 μm (A), 3.5 μm (B). Abbreviations: DAPI, 4′,6-diamidino-2-phenylindole; FISH, fluorescence in situ hybridization; PFA, paraformaldehyde.

3.6. Age-associated increase of tetraploid neurons in the normal human EC

To verify whether dnNT affects specific populations of neurons in the normal human cortex, we focused on its parietal, frontal, and entorhinal areas from a cohort of nondemented individuals with ages ranging from 46 to 76 years. Contrary to the mouse cortex, human parietal and frontal cortices from normal individuals did not show age-associated change in the proportion of tetraploid neurons (Fig. 5A and B). In contrast, the EC, a structure that is first affected in AD (Braak and Braak, 1991), showed a statistically significant, positive correlation with age in the proportion of tetraploid neurons in normal individuals that lack NFTs (Braak stage 0) (Fig. 5C, left panel). When individuals were split according to their age into 2 groups of either below or above 55 years of age, mean values significantly differed by 28% ($p = 9.8 \times 10^{-4}$) (Fig. 5C, right panel). This increase was specific for tetraploid neurons as no net variation with age could be detected in global NeuN-positive cell nuclei (Fig. S13A in Supplementary Material).

3.7. dnNT precedes NFTs in association cortices of AD patients

The presence of dnNT in the EC of nondemented individuals lacking NFTs (see previous section) suggests that this process may precede pathological phosphorylation of Tau protein, as occurs in transgenic mice in which cell cycle re-entry in neurons is forced after simian virus 40 large T antigen expression (Park et al., 2007). To test this hypothesis we focused on the human frontal and parietal cortex of Alzheimer brains at different Braak stages. Since these cortical structures do not undergo age-dependent dnNT (Fig. 5A and B), we defined the proportion of tetraploid neurons in the control situation as the average of the tetraploid neurons present in nonaffected individuals, regardless of their age. Strikingly, the frontal cortex showed a statistically significant increase ($p = 0.027$) in the proportion of tetraploid neurons (NeuN-positive cell nuclei) already at Braak stage II (Fig. 7A), when NFTs are not yet detectable in this structure (Braak and Braak, 1991). In contrast, the proportion of tetraploid neurons (NeuN-positive cell nuclei) in the parietal cortex was not significantly increased until Braak stages V–VI ($p = 0.020$) (Fig. 7B). The increase in the proportion of tetraploid

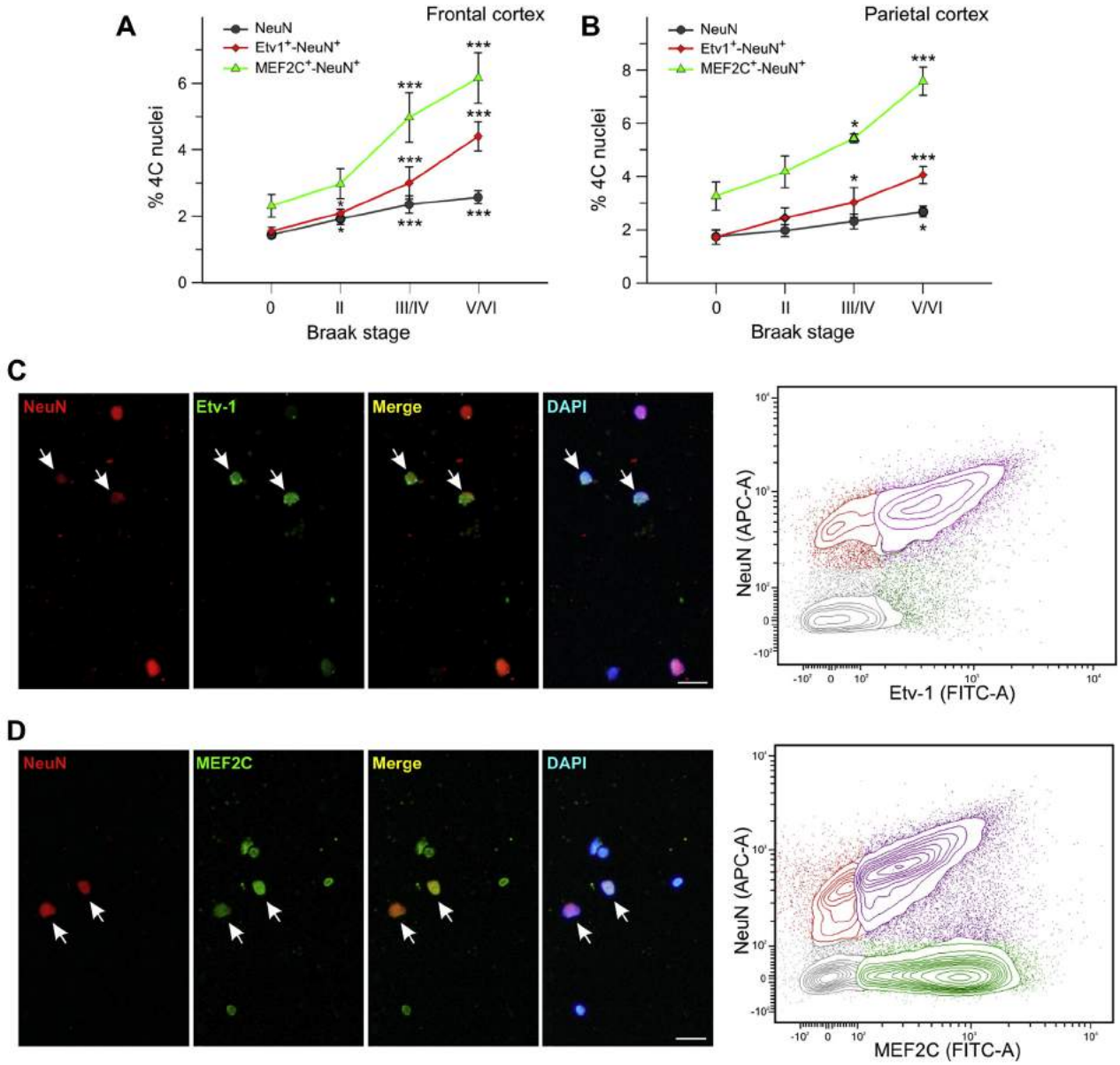

Fig. 7. dnNT precedes NFT formation in the human frontal and parietal cortex. Fresh cell nuclei preparations from frontal (A) and parietal (B) cortices of control individuals (Braak 0) and Alzheimer's disease patients of the indicated Braak stages were immunostained with anti-NeuN to define the whole neuronal population, anti-NeuN plus anti-Etv1 to reveal neurons situated at deep layers (C), or anti-NeuN plus anti-MEF2C antibodies (D). Arrows in left panels from C and D: double-labeled nuclei (revealed with DAPI). Cell nuclei were subsequently labeled with PI, and subjected to flow cytometric analysis (C, D right panels). Double labeled nuclear populations are depicted in purple. The percentage of tetraploid neurons (% 4C nuclei) identified with the different markers was significantly increased both in the frontal (A) and in the parietal (B) cortex. $^{*}p < 0.05$; $^{***}p < 0.005$. Abbreviations: DAPI, 4′,6-diamidino-2-phenylindole; dnNT, de novo-generated neuronal tetraploidy; NFT, neurofibrillary tangle; PI, propidium iodide. (For interpretation of the references to color in this figure legend, the reader is referred to the Web version of this article.)

neurons in these structures was not associated with neuron number alteration as the proportion of NeuN-positive cell nuclei was not significantly changed (p-values in the 0.340–0.858 range) at the Braak stages at which dnNT was evident (Fig. S13B and C in Supplementary Material).

To try to define the phenotype of the neurons that become tetraploid in the frontal and parietal cortex we focused on the laminar markers Etv1/ER81 (hereafter Etv1) and MEF2C. Etv1 was chosen as a marker for cells located in the deep layers (Watakabe et al., 2007; Yoneshima et al., 2006) since, in our hands, different CTIP2-specific antibodies did not label freshly prepared, human cell nuclei from the studied cortical areas. In contrast to the specificity of Etv1 for the cortical layer V in rodents and primates (Watakabe et al., 2007; Yoneshima et al., 2006), this transcription factor was expressed by most cortical neurons located in the deep layers as well as by a small proportion of cortical neurons located in the superficial layers of the human frontal cortex (Fig. S14A in Supplementary Material). Therefore, we concluded that Etv1 is enriched in neurons from the deep layers of the human cerebral cortex. In contrast to the mouse cerebral cortex, MEF2C was detected at high levels in most neurons from both superficial and deep layers of the human cerebral cortex (Fig. S14B in Supplementary Material).

By performing double labeling with NeuN and either Etv1 or MEF2C in fresh cell nuclei isolated from the frontal and parietal cortex (Fig. 7C and D) we confirmed a statistically significant

increase of tetraploid, Etv1-positive neurons ($p = 0.010$) already at Braak stage II in the frontal cortex (Fig. 7A). Furthermore, we could observe a statistically significant increase of tetraploid, Etv1 ($p = 0.035$) and MEF2C ($p = 0.015$) neurons in the parietal cortex, and of tetraploid MEF2C neurons in the frontal cortex ($p = 0.004$) at Braak III–IV (Fig. 7B), when NFTs are not yet detectable in this structure (Braak and Braak, 1991). In addition, we found that the proportion of tetraploid, Etv1 and MEF2C neurons is quite high at Braak V–VI in both frontal and parietal cortices (Fig. 7A and B), reaching the MEF2C-positive population around 6%–8% of all MEF2C-positive neurons. Altogether, these results suggest that dnNT affects to neurons located at least in the deep cortical layers of the human frontal and parietal cortex.

3.8. dnNT is potentiated in APP/PS1 mice

Both amyloid precursor protein (APP) intracellular domain and soluble APP β, 2 major products derived from APP processing, can induce cell cycle progression in different neural systems (Ahn et al., 2008; Baratchi et al., 2012; Caillé et al., 2004). In addition, soluble forms of Aβ have been shown to induce cell cycle reentry in cortical neurons in vitro (Seward et al., 2013; Varvel et al., 2008), and soluble $A\beta_{42}$ is highly enriched in the frontal cortex at early Alzheimer stages, before NFTs can be detected (Näslund et al., 2000). Furthermore, cyclin A and cyclin D expression can be detected in the cerebral cortex of a mouse model of AD prior to Aβ deposition (Varvel et al., 2008). Therefore, we reasoned that pathological APP processing may favor dnNT in these structures. To test this notion in vivo we focused on an AD mouse model in which pathological forms of human APP (APP^{swe}) and PS1 ($PS1^{dE9}$) are expressed under a general neuronal promoter (APP/PS1 mice), thus leading to increased Aβ production (Fernandez et al., 2012). This analysis demonstrated that neuronal tetraploidy is potentiated in APP/PS1 mice (Fig. 8A) even at 2 months of age ($p = 5.4 \times 10^{-4}$), before Aβ deposits can be detected in their brain (Zhang et al., 2012). We therefore, concluded that altered APP processing facilitates AD-associated dnNT.

This conclusion is consistent with the observation that a statistically significant, positive correlation exists between the proportion of tetraploid neurons and Thal phases (i.e., brain Aβ burden) in both frontal and parietal cortices (Fig. S15A and B in Supplementary Material). In addition, a significant correlation was also detected between neuronal tetraploidy levels and neuritic plaque burden in the frontal cortex of Alzheimer patients (Fig. S16A and B in Supplementary Material).

3.9. Aβ-associated dnNT differs from age-associated dnNT

In contrast to age-associated dnNT, tetraploidization of neurons in the APP/PS1 mouse model affects to neurons from the superficial layers ($p = 0.019$, 2 months; $p = 8.4 \times 10^{-4}$, 5 months), as identified by high intensity MEF2C/NeuN labeling, but not to neurons located in deep cortical layers ($p = 0.151$, 2 months; $p = 0.346$, 5 months) (i.e., CTIP2-positive cells) (Fig. 8B and C). This indicates that Alzheimer-associated dnNT in APP/PS1 mice seems to differ from that observed in WT mice in association with age.

4. Discussion

In this study we have shown that a small proportion of neurons located in both superficial and deep layers of the adult cerebral cortex undergo dnNT in the normal mouse brain. We demonstrate that the transcription factor E2F1 is necessary for dnNT occurring in the normal cerebral cortex, and that the lack of dnNT in C57-*E2f1*$^{-/-}$ mice correlates with enhanced memory acquisition and consolidation in these mice. We also show that the human cerebral cortex contains tetraploid neurons and that a small proportion of entorhinal neurons in the normal brain and of frontal and parietal neurons in the Alzheimer brain undergoes dnNT prior to the presence of NTFs in these structures. Finally, we provide evidence that altered APP processing potentiates dnNT in cortical neurons located in the superficial layers of the cerebral cortex of adult mice before Aβ deposits are evident. The observed incidence of dnNT in the cerebral cortex could represent an underestimation of its actual value, given that cell cycle reactivation in adult neurons is known to trigger cell death (Arendt et al., 2010; Busser et al., 1998; Yang et al., 2001, 2003).

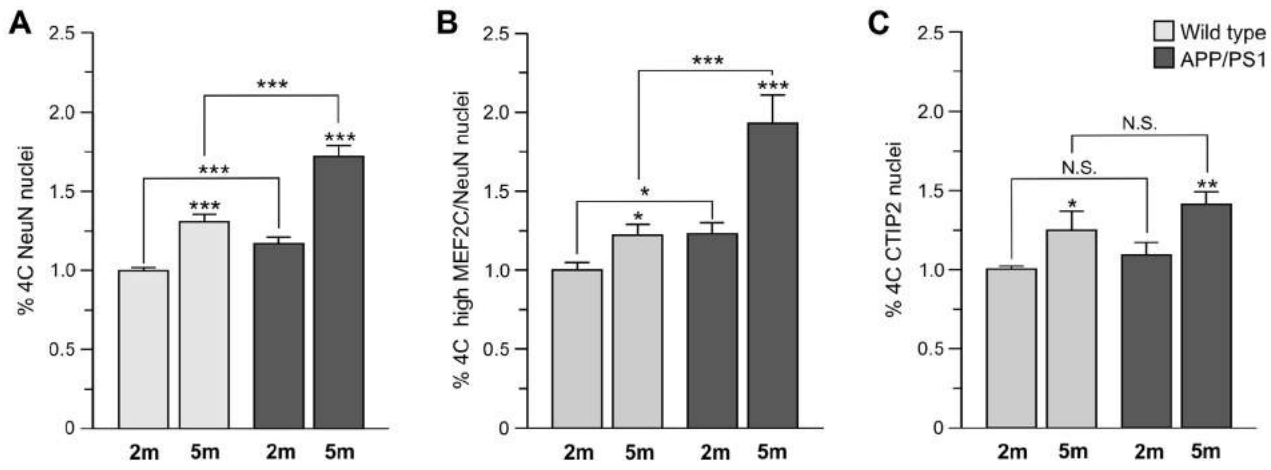

Fig. 8. dnNT is enhanced in the cerebral cortex of APP/PS1 trangenic mice and affects neurons located in the superficial cortical layers. Fresh cell nuclei preparations from cerebral cortex of WT and APP/PS1 transgenic mice of either 2 or 5 months of age were immunostained with anti-NeuN to define the whole neuronal population (A), anti-NeuN plus anti-MEF2C to identify neurons located in the superficial layers (B), or anti-CTIP2 antibodies to reveal projection neurons situated at layers V–VI (C). Cell nuclei were subsequently labeled with PI, and then subjected to flow cytometric analysis. (A) The percentage of tetraploid neurons (% 4C NeuN-positive nuclei) was significantly increased in the cerebral cortex of APP/PS1 transgenic mice at both studied ages. (B) The percentage of tetraploid neurons located in the superficial layers (% 4C high MEF2C/NeuN-positive nuclei) was significantly increased in the cerebral cortex of APP/PS1 transgenic mice at both studied ages. (C) The percentage of tetraploid projection neurons located in layers V–VI (% 4C CTIP2-positive nuclei) was not significantly increased in the cerebral cortex of APP/PS1 transgenic mice at both studied ages. $^{*}p < 0.05$; $^{**}p < 0.01$; $^{***}p < 0.005$. Abbreviations: dnNT, de novo-generated neuronal tetraploidy; N.S. nonsignificant; PI, propidium iodide; APP/PS1, $APP^{swe}/PS1^{deltaE9}$.

4.1. Presence of tetraploid neurons in the adult cerebral cortex

By using a simplified and highly quantitative method developed in our laboratory (López-Sánchez and Frade, 2013a), we have demonstrated that the frontal and parietal cerebral cortex of normal humans contain around 1.5% of neurons with double amount of DNA. We are confident that this method is highly quantitative for a number of reasons. First, it consists of a limited number of steps that avoid differential loss of cell nuclei during the centrifugation (López-Sánchez and Frade, 2013b) and filtering (see Section 2) steps. Second, our protocol uses single nuclei for quantification, as doublets are removed from the analysis using the standard pulse processing method (Nunez, 2001). This issue was confirmed by experiments in which the tetraploid NeuN-positive nuclear population was isolated by FACS. In the isolated tetraploid population, only a minority of events were doublets, likely due to mistakes inherent to the sorting procedure. Third, our flow cytometric method can reveal differences in the proportion of tetraploid neurons when the same tissue is analyzed at the same age in different mouse genetic backgrounds [i.e., WT vs. either C57-*E2f1*$^{-/-}$ (this study) or *p75*$^{NTR-/-}$ mice (López-Sánchez and Frade, 2013a)]. This indicates that the estimated proportion of tetraploid neurons does not derive from either tissue- or age-specific factors. Finally, our results are consistent with the study by Mosch et al. (2007) who, by using SBC, chromogenic in situ hybridization, and real-time polymerase chain reaction amplification of Alu repeats in microdissected neurons, were able to detect a similar range of tetraploid neurons in the EC. Furthermore, we have confirmed by FISH the presence of tetraploid neurons in the human cerebral cortex. This analysis was carried out in PFA-fixed cell nuclei from parietal cortex previously immunolabeled with NeuN-specific antibodies, a procedure that combines NeuN immunolabeling with FISH signal and DAPI staining.

Our procedure seems not to be able to identify neurons with partial chromosomal deletions or duplications (Cai et al., 2014; McConnell et al., 2013) or with aneuploid chromosomal complement (Iourov et al., 2009; Rehen et al., 2001). This is likely due to the relatively low amount of genomic DNA affected in these cases, as compared with the diploid mammalian genome, which in humans consists of above 6000 Mb (International Human Genome Sequencing Consortium, 2004) distributed in 46 chromosomes. McConnell et al. (2013) and Cai et al. (2014) have reported genomic variations below 75 Mb, which represent less than 1% of the genome in a diploid cell. In addition, the impact of a monosomy or trisomy on a diploid genome is also minor (as an average, it would affect around 2% of the genomic DNA present in a diploid human cell). These variations of DNA content are below the coefficient of variation of our technique (6.27% ± 0.17% [$n = 20$] for frontal cortex, 6.40% ± 0.31% [$n = 8$] for parietal cortex, and 6.90% ± 0.17% [$n = 6$] for entorhinal cortex).

Tetraploid neurons cannot be confounded with those showing more than diploid, but not tetraploid DNA content (Arendt et al., 2010; Mosch et al., 2007; Westra et al., 2010) as their nuclei incorporate double amount of PI when analyzed by flow cytometry and they lack under- or over-represented genomic domains when compared with diploid neurons through CGH array analysis. This latter observation is consistent with unpublished results from our laboratory demonstrating that the genome of tetraploid neurons in the mouse cortex has also been homogeneously amplified. Our inability to detect neurons with more than diploid, but not tetraploid DNA content might result from technical constraints of our method. Nevertheless, we note that Westra et al. (2010), Mosch et al. (2007), and Arendt et al. (2010) used fixed material, while our analysis was performed with fresh cell nuclei.

Our observations demonstrating the presence of tetraploid neurons in the frontal and parietal cortex of normal humans are consistent with the presence in different neural structures from other vertebrates of functional tetraploid neurons generated during development (López-Sánchez and Frade, 2013a; López-Sanchez et al., 2011; Morillo et al., 2010; Shirazi Fard et al., 2013, 2014). Therefore, the existence of tetraploid neurons in the normal brain seems to be a common feature of higher vertebrates. Tetraploid neurons would represent a specific form of genomic mosaicism in neurons, also including events of DNA content variation (Bushman et al., 2015; Cai et al., 2014; McConnell et al., 2013; Westra et al., 2010), LINE-1 insertions (Muotri et al., 2005), and aneuploidy (Iourov et al., 2009; Rehen et al., 2001, but see also Knouse et al., 2014 and van den Bos et al., 2016).

4.2. Age-associated dnNT in the normal brain

4.2.1. Age-associated dnNT in the murine cerebral cortex

In this study, we have described for the first time the existence of age-associated, tetraploidization affecting adult neurons in the murine cerebral cortex. This process involves neurons from both superficial and deep cortical layers, an observation that contrasts with the finding that development-associated neuronal tetraploidization preferentially affects to projection neurons located in deep cortical layers (López-Sánchez and Frade, 2013a). This discrepancy suggests that age-associated, dnNT cannot be considered as a mere continuation of the neuronal tetraploidization process taking place during development.

We provide evidence for the participation of E2F1 in age-associated dnNT in the mouse cerebral cortex as this process is completely blocked in C57-*E2f1*$^{-/-}$ mice. This observation is consistent with a previous study showing that E2F1 is expressed by murine cortical neurons, being enriched in an age-dependent fashion (Ting et al., 2014), as well as with our own data indicating that E2F1 can be detected in neurons from mice of 2.5 months of age. Blockade of dnNT in C57-*E2f1*$^{-/-}$ mice is consistent with the known function of E2F1 as a regulator of G1/S transition in proliferating cells (Liu et al., 1998). In this context, postmitotic neurons can reactivate the cell cycle in response to E2F1. This is the case for differentiated photoreceptor cells (Lin et al., 2001), adult rat sensory neurons (Smith et al., 2000), and cerebral cortical neurons coexpressing E2F1 and the viral oncoprotein E1A (Suda et al., 1994).

Our study indicates that dnNT inhibition in C57-*E2f1*$^{-/-}$ mice correlates with improved memory acquisition and consolidation under demanding training conditions in these mice, as evaluated by NOR and MWM tests. In contrast, under standard training conditions, C57-WT mice performed similarly to C57-*E2f1*$^{-/-}$ mice. This effect on memory formation and consolidation, which is already observed at 5 months of age, is unlikely to derive from global changes of E2F1-dependent neuronal plasticity. Indeed, the reduction of synaptic protein levels observed in C57-*E2f1*$^{-/-}$ mice is only evident when these mice are older than 6 months (Ting et al., 2014), an age at which cognitive change is already evident.

Our work contrasts with the study by Ting et al. (2014), which concluded that *E2f1*$^{-/-}$ mice show memory-related deficits. This latter conclusion was based on NOR tests performed under demanding conditions similar to ours (5 minutes training). The reason for this discrepancy is unclear, but we note that Ting et al. (2014) used both *E2f1*$^{-/-}$ and WT mice in a mixed genetic background (C57BL/6 and SV129) whereas our studies were performed with *E2f1*$^{-/-}$ mice in a pure C57BL/6 genetic background (C57-*E2f1*$^{-/-}$ mice). We also note that, in contrast to the observations made by these authors with WT mice, several studies demonstrate that, under similar demanding training conditions, WT mice cannot form and consolidate memory in the object recognition paradigm (see, for instance, Boess et al., 2007; Chopin et al., 2002; Fan et al., 2010; Kikusui et al., 2012). Indeed, these stringent training

protocols are frequently used to study the capacity of specific compounds to improve memory capacity (Boess et al., 2007; Chopin et al., 2002; Fan et al., 2010; Fontán-Lozano et al., 2007, 2008, 2009, 2011a,b; Kikusui et al., 2012). In addition, our MWM test-based analysis performed under demanding acquisition conditions further supports the conclusion that E2F1 disruption prevents the cognitive deficits observed in WT mice.

Our stereological analyses are consistent with previous studies showing reduced adult neurogenesis and death of newly formed neurons in the DG of C57-*E2f1*$^{-/-}$ mice (Cooper-Kuhn et al., 2002; Ting et al., 2014), a phenomenon that is compatible with enhanced cognition in these mice. These analyses also indicate that a quite small, although statistically significant increase of total entorhinal neurons can be detected in 5-month-old C57-*E2f1*$^{-/-}$ mice, which seems to be specific for this structure as other cortical regions such as the MC does not show this effect. Interestingly, this increase of entorhinal neurons was not evident when 1-year-old C57-*E2f1*$^{-/-}$ mice were evaluated. Nevertheless, the behavioral phenotype of C57-*E2f1*$^{-/-}$ mice was similar at both ages, thus suggesting that the observed variation in entorhinal neuron numbers is not related to the results obtained with the cognitive tests.

4.2.2. Age-associated dnNT in the human entorhinal cortex

Our study has revealed a gradual age-associated increase of tetraploid neurons in the human EC, an effect that is specific for this structure as dnNT cannot be detected in frontal and parietal cortices. This process was evaluated in control individuals lacking signs of dementia as well as of NFTs in the EC, a structure that frequently contains phosphoTau deposits in the normal brain (Braak and Del Tredici, 2014). Therefore, age-associated dnNT in the EC seems to precede and be independent from dnNT occurring in the cerebral cortex of AD patients (Mosch et al., 2007; Yang et al., 2001). We speculate that dnNT in the human EC might participate in age-dependent cognitive decline (Singh-Manoux et al., 2012), as entorhinal neurons are known to be involved in memory processing (Squire and Zola-Morgan, 1991).

4.3. dnNT in Alzheimer

Our results provide evidence for the existence of dnNT in the frontal and parietal cortex at very early stages of AD, preceding the onset of NFTs in these structures. This observation is consistent with a previous report focused on hyperploid entorhinal neurons (Arendt et al., 2010). Since NFTs are known to correlate with the severity of dementia in AD patients (Arriagada et al., 1992; Giannakopoulos et al., 2003; Gómez-Isla et al., 1997), we postulate that AD-associated dnNT, which anticipates NFT formation (see previous section), could participate in the cognitive alterations observed in AD patients, as it might occur with age-associated dnNT in WT mice. This notion is consistent with the high variability observed when the levels of dnNT are plotted against Thal stages (Fig. S15). Indeed, cognitive loss (which under our hypothesis would be linked to dnNT) does not to fully correlate with Aβ deposit load (Arriagada et al., 1992; Giannakopoulos et al., 2003; Gómez-Isla et al., 1997).

We provide evidence that the cerebral cortex of transgenic mice expressing pathological forms of human APP and PS1 have increased levels of dnNT even at 2 months of age, prior to the presence of Aβ deposits in their brain (Zhang et al., 2012). This observation is consistent with previous studies reporting loss of neuronal cell cycle control in APP and PS1 transgenic mouse models (Malik et al., 2008; Varvel et al., 2008; Yang et al., 2006), a finding consistent with the participation of APP in cell proliferation of the murine neurepithelium (López-Sánchez et al., 2005). We conclude, therefore, that neuronal tetraploidization precedes the appearance of the main neuropathological hallmarks of AD, both NFTs and SPs.

APP/PS1 mice show enhanced Aβ production, and cumulative evidence indicates that Aβ oligomers are major players in AD development (Varvel et al., 2008; Viola and Klein, 2015). Therefore, it is likely that the presence of soluble Aβ oligomers in the cerebral cortex of 2-month-old APP/PS1 mice (Tanghe et al., 2010) could potentiate cell cycle reentry in cortical neurons, as previously shown in vitro (Seward et al., 2013; Varvel et al., 2008). In turn, dnNT may lead to enhanced Aβ production (Park et al., 2007), thus participating in the spatial expansion of the disease.

Pathological APP processing results in the concomitant production of APP intracellular domain and soluble APP-β, 2 proteins known to trigger proliferative effects in different neural systems (Ahn et al., 2008; Baratchi et al., 2012; Caillé et al., 2004). This suggests that a multiplicity of proliferative signals that may trigger dnNT could be activated upon APP cleavage in AD. Since forced cell cycle reentry in neurons has been shown to lead to tau hyperphosphorylation (Park et al., 2007), it is tempting to speculate that dnNT could facilitate NFTs formation in AD. Therefore, dnNT blockade might be crucial for an effectively treatment of AD if this hypothesis turns out to be true.

In contrast with our observation that AD-associated, dnNT seems to affect to neurons located at least in deep cortical layers, dnNT in APP/PS1 mice specifically affected to superficial layer neurons. This suggests that dnNT occurring in the deep cortical layers in AD may be triggered as a secondary wave of dnNT, as suggested by Varvel et al. (2008).

5. Conclusions

Our study provides evidence for the existence of dnNT in both normal and Alzheimer brain. Since dnNT represents a dynamic process occurring in adult neurons, it is unlikely to derive from mitotic errors during development, as those described by Rehen et al. (2001). Nevertheless, it still remains to be clarified whether dnNT is due to unscheduled cell cycle activation in neurons or just to defects in DNA repair. In this regard, our data rather suggests that the mechanism triggering dnNT seems to be associated with the activation of the cell cycle since this process can be blocked in the absence of E2F1 and it ends up with the full duplication of the genome in differentiated neurons.

Our study provides evidence that dnNT in both normal and Alzheimer brain precedes and correlates with alterations in cognitive function, thus suggesting that dnNT may be part of the regressive events associated with brain maturation, aging, and neurodegenerative diseases. It will be important to understand the pathophysiological effects induced by dnNT in the affected adult neurons as well as in the neuronal networks in which these neurons are integrated. This knowledge will surely provide crucial information for our understanding of age-associated brain alterations. The correlation of dnNT with cognitive decline and its spatiotemporal course, preceding and recapitulating Alzheimer-associated neuropathology, makes this process a potential target for intervention in AD.

Disclosure statement

J. M. F. is shareholder of Tetraneuron S. L. (10% equity ownership). N. L. S. has received her salary from an R&D contract with Tetraneuron S. L. and currently works for Tetraneuron S. L. The other authors report no conflicts of interest.

Acknowledgements

The authors thank Álvaro Gómez-Jiménez for his participation in E2F1 expression analysis and María J. Alonso for her technical help.

This work was supported by the Ministerio de Economía y Competitividad [grant numbers SAF2012-38316 (J. M. F.), SAF2015-68488-R (J. M. F.), BFU2013-48907-R (J. L. T.)]; and an R&D contract with Tetraneuron S. L. (J. M. F.).

Appendix A. Supplementary data

Supplementary data associated with this article can be found, in the online version, at http://dx.doi.org/10.1016/j.neurobiolaging.2017.04.008.

References

Ahn, K.W., Joo, Y., Choi, Y., Kim, M., Lee, S.H., Cha, S.H., Suh, Y.H., Kim, H.S., 2008. Swedish amyloid precursor protein mutation increases cell cycle-related proteins in vitro and in vivo. J. Neurosci. Res. 86, 2476–2487.

Arendt, T., Brückner, M.K., Mosch, B., Lösche, A., 2010. Selective cell death of hyperploid neurons in Alzheimer's disease. Am. J. Pathol. 177, 15–20.

Arlotta, P., Molyneaux, B.J., Chen, J., Inoue, J., Kominami, R., Macklis, J.D., 2005. Neuronal subtype-specific genes that control corticospinal motor neuron development in vivo. Neuron 45, 207–221.

Arriagada, P.V., Growdon, J.H., Hedley-Whyte, E.T., Hyman, B.T., 1992. Neurofibrillary tangles but not senile plaques parallel duration and severity of Alzheimer's disease. Neurology 42, 631–639.

Baratchi, S., Evans, J., Tate, W.P., Abraham, W.C., Connor, B., 2012. Secreted amyloid precursor proteins promote proliferation and glial differentiation of adult hippocampal neural progenitor cells. Hippocampus 22, 1517–1527.

Boess, F.G., De Vry, J., Erb, C., Flessner, T., Hendrix, M., Luithle, J., Methfessel, C., Riedl, B., Schnizler, K., van der Staay, F.J., van Kampen, M., Wiese, W.B., Koenig, G., 2007. The novel α7 nicotinic acetylcholine receptor agonist N-[(3R)-1-azabicyclo[2.2.2]oct-3-yl]-7-[2-(methoxy)phenyl]-1-benzofuran-2-carboxamide improves working and recognition memory in rodents. J. Pharmacol. Exp. Ther. 321, 716–725.

Bowser, R., Smith, M.A., 2002. Cell cycle proteins in Alzheimer's disease: plenty of wheels but no cycle. J. Alzheimers Dis. 4, 249–254.

Braak, H., Braak, E., 1991. Neuropathological staging of Alzheimer-related changes. Acta Neuropathol. 82, 239–259.

Braak, H., Del Tredici, K., 2014. Are cases with tau pathology occurring in the absence of Aβ deposits part of the AD-related pathological process? Acta Neuropathol. 128, 767–772.

Brandt, M.D., Jessberger, S., Steiner, B., Kronenberg, G., Reuter, K., Bick-Sander, A., von der Behrens, W., Kempermann, G., 2003. Transient calretinin expression defines early postmitotic step of neuronal differentiation in adult hippocampal neurogenesis of mice. Mol. Cell Neurosci. 24, 603–613.

Brookmeyer, R., Gray, S., Kawas, C., 1998. Projections of Alzheimer's disease in the United States and the public health impact of delaying disease onset. Am. J. Public Health 88, 1337–1342.

Bushman, D.M., Kaeser, G.E., Siddoway, B., Westra, J.W., Rivera, R.R., Rehen, S.K., Yung, Y.C., Chun, J., 2015. Genomic mosaicism with increased amyloid precursor protein (APP) gene copy number in single neurons from sporadic Alzheimer's disease brains. Elife 4.

Busser, J., Geldmacher, D.S., Herrup, K., 1998. Ectopic cell cycle proteins predict the sites of neuronal cell death in Alzheimer's disease brain. J. Neurosci. 18, 2801–2807.

Cai, X., Evrony, G.D., Lehmann, H.S., Elhosary, P.C., Mehta, B.K., Poduri, A., Walsh, C.A., 2014. Single-cell, genome-wide sequencing identifies clonal somatic copy-number variation in the human brain. Cell Rep. 8, 1280–1289.

Caillé, I., Allinquant, B., Dupont, E., Bouillot, C., Langer, A., Müller, U., Prochiantz, A., 2004. Soluble form of amyloid precursor protein regulates proliferation of progenitors in the adult subventricular zone. Development 131, 2173–2181.

Chaumeil, J., Micsinai, M., Skok, J.A., 2013. Combined immunofluorescence and DNA FISH on 3D-preserved interphase nuclei to study changes in 3D nuclear organization. J. Vis. Exp. e50087.

Chopin, P., Colpaert, F.C., Marien, M., 2002. Effects of acute and subchronic administration of dexefaroxan, an α_2-adrenoceptor antagonist, on memory performance in young adult and aged rodents. J. Pharmacol. Exp. Ther. 301, 187–196.

Cooper-Kuhn, C.M., Vroemen, M., Brown, J., Ye, H., Thompson, M.A., Winkler, J., Kuhn, H.G., 2002. Impaired adult neurogenesis in mice lacking the transcription factor E2F1. Mol. Cell Neurosci. 21, 312–323.

Ding, X.L., Husseman, J., Tomashevski, A., Nochlin, D., Jin, L.W., Vincent, I., 2000. The cell cycle Cdc25A tyrosine phosphatase is activated in degenerating postmitotic neurons in Alzheimer's disease. Am. J. Pathol. 157, 1983–1990.

Ennaceur, A., Delacour, J., 1988. A new one-trial test for neurobiological studies of memory in rats. 1: behavioral data. Behav. Brain Res. 31, 47–59.

Fan, L., Zhao, Z., Orr, P.T., Chambers, C.H., Lewis, M.C., Frick, K.M., 2010. Estradiol-induced object memory consolidation in middle-aged female mice requires dorsal hippocampal extracellular signal-regulated kinase and phosphatidylinositol 3-kinase activation. J. Neurosci. 30, 4390–4400.

Fernandez, A.M., Jimenez, S., Mecha, M., Dávila, D., Guaza, C., Vitorica, J., Torres-Aleman, I., 2012. Regulation of the phosphatase calcineurin by insulin-like growth factor I unveils a key role of astrocytes in Alzheimer's pathology. Mol. Psychiatry 17, 705–718.

Field, S.J., Tsai, F.Y., Kuo, F., Zubiaga, A.M., Kaelin Jr., W.G., Livingston, D.M., Orkin, S.H., Greenberg, M.E., 1996. E2F-1 functions in mice to promote apoptosis and suppress proliferation. Cell 85, 549–561.

Fontán-Lozano, A., Romero-Granados, R., del-Pozo-Martín, Y., Suárez-Pereira, I., Delgado-García, J.M., Penninger, J.M., Carrión, A.M., 2009. Lack of DREAM protein enhances learning and memory and slows brain aging. Curr. Biol. 19, 54–60.

Fontán-Lozano, A., Romero-Granados, R., Troncoso, J., Múnera, A., Delgado-García, J.M., Carrión, A.M., 2008. Histone deacetylase inhibitors improve learning consolidation in young and in KA-induced-neurodegeneration and SAMP-8-mutant mice. Mol. Cell Neurosci. 39, 193–201.

Fontán-Lozano, A., Sáez-Cassanelli, J.L., Inda, M.C., de los Santos-Arteaga, M., Sierra-Domínguez, S.A., López-Lluch, G., Delgado-García, J.M., Carrión, A.M., 2007. Caloric restriction increases learning consolidation and facilitates synaptic plasticity through mechanisms dependent on NR2B subunits of the NMDA receptor. J. Neurosci. 27, 10185–10195.

Fontán-Lozano, A., Suárez-Pereira, I., Delgado-García, J.M., Carrión, A.M., 2011a. The M-current inhibitor XE991 decreases the stimulation threshold for long-term synaptic plasticity in healthy mice and in models of cognitive disease. Hippocampus 21, 22–32.

Fontán-Lozano, Á., Suárez-Pereira, I., González-Forero, D., Carrión, A.M., 2011b. The A-current modulates learning via NMDA receptors containing the NR2B subunit. PLoS One 6, e24915.

Förstl, H., Kurz, A., 1999. Clinical features of Alzheimer's disease. Eur. Arch. Psychiatry Clin. Neurosci. 249, 288–290.

Frade, J.M., López-Sánchez, N., 2010. A novel hypothesis for Alzheimer disease based on neuronal tetraploidy induced by $p75^{NTR}$. Cell Cycle 9, 1934–1941.

Giannakopoulos, P., Herrmann, F.R., Bussière, T., Bouras, C., Kövari, E., Perl, D.P., Morrison, J.H., Gold, G., Hof, P.R., 2003. Tangle and neuron numbers, but not amyloid load, predict cognitive status in Alzheimer's disease. Neurology 60, 1495–1500.

Gómez-Isla, T., Hollister, R., West, H., Mui, S., Growdon, J.H., Petersen, R.C., Parisi, J.E., Hyman, B.T., 1997. Neuronal loss correlates with but exceeds neurofibrillary tangles in Alzheimer's disease. Ann. Neurol. 41, 17–24.

Hoozemans, J.J., Brückner, M.K., Rozemuller, A.J., Veerhuis, R., Eikelenboom, P., Arendt, T., 2002. Cyclin D1 and cyclin E are co-localized with cyclo-oxygenase 2 (COX-2) in pyramidal neurons in Alzheimer disease temporal cortex. J. Neuropathol. Exp. Neurol. 61, 678–688.

International Human Genome Sequencing Consortium, 2004. Finishing the euchromatic sequence of the human genome. Nature 431, 931–945.

Iourov, I.Y., Vorsanova, S.G., Liehr, T., Yurov, Y.B., 2009. Aneuploidy in the normal, Alzheimer's disease and ataxia-telangiectasia brain: differential expression and pathological meaning. Neurobiol. Dis. 34, 212–220.

Jordan-Sciutto, K.L., Malaiyandi, L.M., Bowser, R., 2002. Altered distribution of cell cycle transcriptional regulators during Alzheimer disease. J. Neuropathol. Exp. Neurol. 61, 358–367.

Kikusui, T., Shimozawa, A., Kitagawa, A., Nagasawa, M., Mogi, K., Yagi, S., Shiota, K., 2012. N-acetylmannosamine improves object recognition and hippocampal cell proliferation in middle-aged mice. Biosci. Biotechnol. Biochem. 76, 2249–2254.

Knouse, K.A., Wu, J., Whittaker, C.A., Amon, A., 2014. Single cell sequencing reveals low levels of aneuploidy across mammalian tissues. Proc. Natl. Acad. Sci. U. S. A. 111, 13409–13414.

Leifer, D., Krainc, D., Yu, Y.T., McDermott, J., Breitbart, R.E., Heng, J., Neve, R.L., Kosofsky, B., Nadal-Ginard, B., Lipton, S.A., 1993. MEF2C, a MADS/MEF2-family transcription factor expressed in a laminar distribution in cerebral cortex. Proc. Natl. Acad. Sci. U. S. A. 90, 1546–1550.

Lin, S.C., Skapek, S.X., Papermaster, D.S., Hankin, M., Lee, E.Y., 2001. The proliferative and apoptotic activities of E2F1 in the mouse retina. Oncogene 20, 7073–7084.

Liu, N., Lucibello, F.C., Engeland, K., Müller, R., 1998. A new model of cell cycle-regulated transcription: repression of the cyclin A promoter by CDF-1 and anti-repression by E2F. Oncogene 16, 2957–2963.

Llorens-Martín, M., Torres-Alemán, I., Trejo, J.L., 2006. Pronounced individual variation in the response to the stimulatory action of exercise on immature hippocampal neurons. Hippocampus 16, 480–490.

López-Sánchez, N., Frade, J.M., 2013a. Genetic evidence for $p75^{NTR}$-dependent tetraploidy in cortical projection neurons from adult mice. J. Neurosci. 33, 7488–7500.

López-Sánchez, N., Frade, J.M., 2013b. Cell cycle analysis in the vertebrate brain using immunolabeled fresh cell nuclei. Bio Protoc. 3, e973.

López-Sánchez, N., Frade, J.M., 2015. Flow cytometric analysis of DNA synthesis and apoptosis in central nervous system using fresh cell nuclei. Methods Mol. Biol. 1254, 33–42.

López-Sánchez, N., Müller, U., Frade, J.M., 2005. Lengthening of G2/mitosis in cortical precursors from mice lacking beta-amyloid precursor protein. Neuroscience 130, 51–60.

López-Sánchez, N., Ovejero-Benito, M.C., Borreguero, L., Frade, J.M., 2011. Control of neuronal ploidy during vertebrate development. Results Probl. Cell Differ. 53, 547–563.

Malik, B., Currais, A., Andres, A., Towlson, C., Pitsi, D., Nunes, A., Niblock, M., Cooper, J., Hortobágyi, T., Soriano, S., 2008. Loss of neuronal cell cycle control as a mechanism of neurodegeneration in the presenilin-1 Alzheimer's disease brain. Cell Cycle 7, 637–646.

Markesbery, W.R., 1997. Neuropathological criteria for the diagnosis of Alzheimer's disease. Neurobiol. Aging 18, S13–S19.
McConnell, M.J., Lindberg, M.R., Brennand, K.J., Piper, J.C., Voet, T., Cowing-Zitron, C., Shumilina, S., Lasken, R.S., Vermeesch, J.R., Hall, I.M., Gage, F.H., 2013. Mosaic copy number variation in human neurons. Science 342, 632–637.
McShea, A., Harris, P.L., Webster, K.R., Wahl, A.F., Smith, M.A., 1997. Abnormal expression of the cell cycle regulators P16 and CDK4 in Alzheimer's disease. Am. J. Pathol. 150, 1933–1939.
Montine, T.J., Phelps, C.H., Beach, T.G., Bigio, E.H., Cairns, N.J., Dickson, D.W., Duyckaerts, C., Frosch, M.P., Masliah, E., Mirra, S.S., Nelson, P.T., Schneider, J.A., Thal, D.R., Trojanowski, J.Q., Vinters, H.V., Hyman, B.T. National Institute on Aging Alzheimer's Association, 2012. National Institute on Aging-Alzheimer's Association guidelines for the neuropathologic assessment of Alzheimer's disease: a practical approach. Acta Neuropathol. 123, 1–11.
Morillo, S.M., Abanto, E.P., Román, M.J., Frade, J.M., 2012. Nerve growth factor-induced cell cycle reentry in newborn neurons is triggered by $p38^{MAPK}$-dependent E2F4 phosphorylation. Mol. Cell Biol. 32, 2722–2737.
Morillo, S.M., Escoll, P., de la Hera, A., Frade, J.M., 2010. Somatic tetraploidy in specific chick retinal ganglion cells induced by nerve growth factor. Proc. Natl. Acad. Sci. U. S. A. 107, 109–114.
Morris, R.G.M., 1981. Spatial localization does not require the presence of local cues. Learn Motiv. 12, 239–260.
Mosch, B., Morawski, M., Mittag, A., Lenz, D., Tarnok, A., Arendt, T., 2007. Aneuploidy and DNA replication in the normal human brain and Alzheimer's disease. J. Neurosci. 27, 6859–6867.
Mullen, R.J., Buck, C.R., Smith, A.M., 1992. NeuN, a neuronal specific nuclear protein in vertebrates. Development 116, 201–211.
Muotri, A.R., Chu, V.T., Marchetto, M.C., Deng, W., Moran, J.V., Gage, F.H., 2005. Somatic mosaicism in neuronal precursor cells mediated by L1 retrotransposition. Nature 435, 903–910.
Nagy, Z., Esiri, M.M., Cato, A.M., Smith, A.D., 1997. Cell cycle markers in the hippocampus in Alzheimer's disease. Acta Neuropathol. 94, 6–15.
Näslund, J., Haroutunian, V., Mohs, R., Davis, K.L., Davies, P., Greengard, P., Buxbaum, J.D., 2000. Correlation between elevated levels of amyloid β-peptide in the brain and cognitive decline. JAMA 283, 1571–1577.
Nunez, R., 2001. DNA measurement and cell cycle analysis by flow cytometry. Curr. Issues Mol. Biol. 3, 67–70.
Park, K.H., Hallows, J.L., Chakrabarty, P., Davies, P., Vincent, I., 2007. Conditional neuronal simian virus 40 T antigen expression induces Alzheimer-like tau and amyloid pathology in mice. J. Neurosci. 27, 2969–2978.
Rehen, S.K., McConnell, M.J., Kaushal, D., Kingsbury, M.A., Yang, A.H., Chun, J., 2001. Chromosomal variation in neurons of the developing and adult mammalian nervous system. Proc. Natl. Acad. Sci. U. S. A. 98, 13361–13366.
Seward, M.E., Swanson, E., Norambuena, A., Reimann, A., Cochran, J.N., Li, R., Roberson, E.D., Bloom, G.S., 2013. Amyloid-β signals through tau to drive ectopic neuronal cell cycle re-entry in Alzheimer's disease. J. Cell Sci. 126, 1278–1286.
Shirazi Fard, S., All-Ericsson, C., Hallböök, F., 2014. The heterogenic final cell cycle of chicken retinal Lim1 horizontal cells is not regulated by the DNA damage response pathway. Cell Cycle 13, 408–417.
Shirazi Fard, S., Jarrin, M., Boije, H., Fillon, V., All-Eriksson, C., Hallböök, F., 2013. Heterogenic final cell cycle by chicken retinal Lim1 horizontal progenitor cells leads to heteroploid cells with a remaining replicated genome. PLoS One 8, e59133.
Singh-Manoux, A., Kivimaki, M., Glymour, M.M., Elbaz, A., Berr, C., Ebmeier, K.P., Ferrie, J.E., Dugravot, A., 2012. Timing of onset of cognitive decline: results from Whitehall II prospective cohort study. BMJ 344, d7622.
Smith, D.S., Leone, G., DeGregori, J., Ahmed, M.N., Qumsiyeh, M.B., Nevins, J.R., 2000. Induction of DNA replication in adult rat neurons by deregulation of the retinoblastoma/E2F G1 cell cycle pathway. Cell Growth Differ. 11, 625–633.
Smith, T.W., Lippa, C.F., 1995. Ki-67 immunoreactivity in Alzheimer's disease and other neurodegenerative disorders. J. Neuropathol. Exp. Neurol. 54, 297–303.
Squire, L.R., Zola-Morgan, S., 1991. The medial temporal lobe memory system. Science 253, 1380–1386.
Suda, K., Holmberg, E.G., Nornes, H.O., Neuman, T., 1994. DNA synthesis is induced in adult neurons after expression of E2F1 and E1A. Neuroreport 5, 1749–1751.
Sultana, R., Butterfield, D.A., 2007. Regional expression of key cell cycle proteins in brain from subjects with amnestic mild cognitive impairment. Neurochem. Res. 32, 655–662.
Tanghe, A., Termont, A., Merchiers, P., Schilling, S., Demuth, H.U., Scrocchi, L., Van Leuven, F., Griffioen, G., Van Dooren, T., 2010. Pathological hallmarks, clinical parallels, and value for drug testing in Alzheimer's disease of the APP[V717I] London transgenic mouse model. Int. J. Alzheimers Dis. 2010, 417314.
Thakur, A., Siedlak, S.L., James, S.L., Bonda, D.J., Rao, A., Webber, K.M., Camins, A., Pallàs, M., Casadesus, G., Lee, H.G., Bowser, R., Raina, A.K., Perry, G., Smith, M.A., Zhu, X., 2008. Retinoblastoma protein phosphorylation at multiple sites is associated with neurofibrillary pathology in Alzheimer disease. Int. J. Clin. Exp. Pathol. 1, 134–146.
Thal, D.R., Rüb, U., Orantes, M., Braak, H., 2002. Phases of A beta-deposition in the human brain and its relevance for the development of AD. Neurology 58, 1791–1800.
Thal, D.R., Rüb, U., Schultz, C., Sassin, I., Ghebremedhin, E., Del Tredici, K., Braak, E., Braak, H., 2000. Sequence of Abeta-protein deposition in the human medial temporal lobe. J. Neuropathol. Exp. Neurol. 59, 733–748.
Ting, J.H., Marks, D.R., Schleidt, S.S., Wu, J.N., Zyskind, J.W., Lindl, K.A., Blendy, J.A., Pierce, R.C., Jordan-Sciutto, K.L., 2014. Targeted gene mutation of E2F1 evokes age-dependent synaptic disruption and behavioral deficits. J. Neurochem. 129, 850–863.
Tomashevski, A., Husseman, J., Jin, L.W., Nochlin, D., Vincent, I., 2001. Constitutive Wee1 activity in adult brain neurons with M phase-type alterations in Alzheimer neurodegeneration. J. Alzheimers Dis. 3, 195–207.
van den Bos, H., Spierings, D.C., Taudt, A.S., Bakker, B., Porubský, D., Falconer, E., Novoa, C., Halsema, N., Kazemier, H.G., Hoekstra-Wakker, K., Guryev, V., den Dunnen, W.F., Foijer, F., Tatché, M.C., Boddeke, H.W., Lansdorp, P.M., 2016. Single-cell whole genome sequencing reveals no evidence for common aneuploidy in normal and Alzheimer's disease neurons. Genome Biol. 17, 116.
Varvel, N.H., Bhaskar, K., Patil, A.R., Pimplikar, S.W., Herrup, K., Lamb, B.T., 2008. Aβ oligomers induce neuronal cell cycle events in Alzheimer's disease. J. Neurosci. 28, 10786–10793.
Vincent, I., Bu, B., Hudson, K., Husseman, J., Nochlin, D., Jin, L., 2001. Constitutive Cdc25B tyrosine phosphatase activity in adult brain neurons with M phase-type alterations in Alzheimer's disease. Neuroscience 105, 639–650.
Vincent, I., Zheng, J.H., Dickson, D.W., Kress, Y., Davies, P., 1998. Mitotic phosphoepitopes precede paired helical filaments in Alzheimer's disease. Neurobiol. Aging 19, 287–296.
Viola, K.L., Klein, W.L., 2015. Amyloid β oligomers in Alzheimer's disease pathogenesis, treatment, and diagnosis. Acta Neuropathol. 129, 183–206.
Watakabe, A., Ichinohe, N., Ohsawa, S., Hashikawa, T., Komatsu, Y., Rockland, K.S., Yamamori, T., 2007. Comparative analysis of layer-specific genes in mammalian neocortex. Cereb. Cortex 17, 1918–1933.
Westra, J.W., Barral, S., Chun, J., 2009. A reevaluation of tetraploidy in the Alzheimer's disease brain. Neurodegener. Dis. 6, 221–229.
Westra, J.W., Rivera, R.R., Bushman, D.M., Yung, Y.C., Peterson, S.E., Barral, S., Chun, J., 2010. Neuronal DNA content variation (DCV) with regional and individual differences in the human brain. J. Comp. Neurol. 518, 3981–4000.
Wolf, H.K., Buslei, R., Schmidt-Kastner, R., Schmidt-Kastner, P.K., Pietsch, T., Wiestler, O.D., Blómcke, I., 1996. NeuN: a useful neuronal marker for diagnostic histopathology. J. Histochem. Cytochem. 44, 1167–1171.
Yang, Y., Geldmacher, D.S., Herrup, K., 2001. DNA replication precedes neuronal cell death in Alzheimer's disease. J. Neurosci. 21, 2661–2668.
Yang, Y., Mufson, E.J., Herrup, K., 2003. Neuronal cell death is preceded by cell cycle events at all stages of Alzheimer's disease. J. Neurosci. 23, 2557–2563.
Yang, Y., Varvel, N.H., Lamb, B.T., Herrup, K., 2006. Ectopic cell cycle events link human Alzheimer's disease and amyloid precursor protein transgenic mouse models. J. Neurosci. 26, 775–784.
Yoneshima, H., Yamasaki, S., Voelker, C.C., Molnær, Z., Christophe, E., Audinat, E., Takemoto, M., Nishiwaki, M., Tsuji, S., Fujita, I., Yamamoto, N., 2006. Er81 is expressed in a subpopulation of layer 5 neurons in rodent and primate neocortices. Neuroscience 137, 401–412.
Zhang, W., Bai, M., Xi, Y., Hao, J., Zhang, Z., Su, C., Lei, G., Miao, J., Li, Z., 2012. Multiple inflammatory pathways are involved in the development and progression of cognitive deficits in $APP^{swe}/PS1^{dE9}$ mice. Neurobiol. Aging 33, 2661–2677.